AIMS Mathematics, 11(1): 366–398.
DOI: 10.3934/math.2026016
Received: 10 October 2025
Revised: 27 November 2025
Accepted: 08 December 2025
Published: 05 January 2026

https://www.aimspress.com/journal/Math

Research article

Predefined-time and finite-time synchronization control of fuzzy Cohen-Grossberg neural networks with two additive time-varying delay

Teng Dong[1] **and Minghui Jiang**[2,*]

[1] College of Mathematical and Physics, China Three Gorges University, Yichang, Hubei, 443002, China

[2] College of Science, China Three Gorges University, Yichang, Hubei, 443000, China

* **Correspondence:** Email: jiangminghui@ctgu.edu.cn.

Abstract: This paper investigated novel predefined-time stability theorems for time-delayed fuzzy Cohen-Grossberg neural networks. A novel predefined-time stability lemma was introduced via a newly developed inequality-based analytical framework.The theoretical results demonstrated that, compared to existing stability criteria in the literature, is provided more precise estimation of settling time boundaries, but also effectively reduced conservatism. To validate the effectiveness of the proposed lemma, the stability theorem was applied to the synchronization control problem of fuzzy Cohen-Grossberg neural networks (FCGNNs).To address this, an adaptive control strategy was proposed, employing a discontinuous state-feedback approach for the response neural network. Rigorous algebraic criteria was established to ensure synchronization within the specified time frame, in line with prior discussions. The effectiveness of the proposed synchronization method was empirically verified through numerical case studies.

Keywords: predefined-time synchronization; fixed-time synchronization; fuzzy Cohen-Grossberg neural networks; additive time-varying delay
Mathematics Subject Classification: 93D21, 93D40

1. Introduction

1.1. Literature review

Building upon conventional cellular neural networks, Yang and Yang [1] first proposed fuzzy cellular neural networks in 1996 to address uncertainty in cognitive processes and improve practical applications including pattern recognition. Later studies primarily focused on delayed fuzzy neural netwaorks (FCNN) variants.

An analysis of existing literature reveals that most studies concerning the stability and synchronization of fuzzy neural networks have been predicated on the assumptions of continuous, Lipschitz continuous, or smooth activation functions. In practical implementations, however, neuronal activation functions frequently demonstrate jump discontinuities with respect to system states. Inspired by the pioneering work of Forti and Nistri [2], researchers in recent years have progressively redirected their attention to neural network systems incorporating discontinuous activation functions. As a representative study, Abdujelil [3] conducted an in-depth investigation into the synchronization of memristor-based Cohen-Grossberg neural networks incorporating mixed time delays and discontinuous activation functions. Their methodology integrated multiple analytical tools including Filippov solutions, differential inclusion theory, Lyapunov-Krasovskii functionals, and diverse inequality techniques. Building upon this foundation, Duan and colleagues [4] made significant advancements by examining finite-time synchronization in delayed fuzzy cellular neural networks with discontinuous activation functions, employing a novel discontinuous state feedback control strategy.

The stability of Filippov discontinuous systems (FDSs) has emerged as a significant area of research, owing not only to their increasing applications in fields such as neuroscience and engineering involving discontinuous systems, but also due to the potential of discontinuities to compromise system stability. Early studies in this domain highlighted the challenges in analyzing the stability of FDSs, primarily due to the lack of suitable theoretical methods. Furthermore, traditional theories, particularly those concerning the existence of solutions, are not applicable to FDSs. Given the presence of discontinuities, instability is an inherent characteristic of these systems, and this issue becomes even more complex when the traditional Lipschitz condition cannot be applied to stability analysis. This challenge was addressed by Polyakov in 2012 [5], who employed differential inclusion theory, developed by Filippov in [6], to handle discontinuities. Polyakov introduced an implicit Lyapunov function to investigate fixed-time (FIXT) stability, making a pioneering contribution by establishing the first FIXT stability lemmas and results for FDSs. This advancement has led to the Lyapunov method becoming an essential tool for studying FIXT stability in FDSs. In recent years, several notable studies, such as [7,8], have further explored the FIXT stability of FDSs. Despite the significant progress made in FIXT stability analysis for discontinuous systems and neural networks, there remains room for improvement in the existing stability lemmas. For instance, the conditions imposed on Lyapunov-Krasovskii functionals (LKF) could be relaxed, and the precision of the stability criteria could be enhanced.

Time delays are prevalent in natural processes and numerous industrial systems, including chemical, biological, and networked control systems, often considered a primary cause of instability. Given the critical role of stability in various systems, extensive research has been conducted in recent years to analyze the stability of time-delay systems. Some models assume the delay appears in a singular or simplified form, as discussed in [9, 10]. However, as noted in [11], multiple delays with distinct characteristics may coexist in certain practical scenarios. Moreover, in networked control systems, the lower bound of time delays is typically nonzero, and the delay may vary within a specific interval. Consequently, stability analysis for systems with interval time-varying delays has attracted significant attention [12, 13]. Nevertheless, limited research has addressed the stability problem for interval time-delay systems involving two additive delay components. The current investigation focuses on addressing robust finite-time and fixed-time synchronization control challenges in fuzzy Cohen-Grossberg neural networks (FCGNNs) featuring time-varying delays and discontinuous activation

functions. To methodically address these issues, the Filippov solution framework is adopted to handle the dynamical behavior of discontinuous systems.

Significant progress has been made in recent years regarding finite-time/fixed-time synchronization control for time-delay neural networks and multi-agent systems.For fuzzy neural networks, Abdurahman et al.established a theoretical framework for finite-time synchronization in fuzzy cellular neural networks with time-varying delays [14]. As control objectives have become more precise, predefined-time synchronization has emerged as a new direction.Lv et al.proposed an output-feedback predefined-time leader-following consensus protocol for pure-feedback multi-agent systems [15]. Meanwhile, Li et al. further investigated the adaptive consensus problem for uncertain multi-agent systems with unified prescribed performance [16]. For nonlinear systems, Lv et al. addressed the leader-following consensus of nonlinear multi-agent systems via a distributed output-feedback approach [17]. In terms of methodological innovation, You et al.applied the maximum-valued method of functions of five variables to achieve finite-time synchronization of fractional-order chaotic systems [18]. For more challenging discontinuous systems, Zhang et al.realized fixed-time stabilization and synchronization of delayed discontinuous inertial neural networks based on aperiodically semi-intermittent control [19]. These achievements provide an important theoretical foundation for the present study on prescribed finite-time and fixed-time synchronization control of fuzzy Cohen-Grossberg neural networks with two additive time-varying delays.

1.2. Outline of this paper

This study focuses on examining synchronization control within predefined-time and fixed-time horizons for FCGNNs featuring time-varying delays and discontinuous activation characteristics. To methodically overcome these technical difficulties, the Filippov solution framework is initially adopted to address the discontinuous righthand terms in the system equations. This paper develops an enhanced predefined-time stability lemma applicable to discontinuous dynamical systems, which provides improved accuracy in estimating the required convergence time. Building upon this novel stability lemma, we further derive sufficient conditions for achieving predefined-time stability in FCGNNs with discontinuous activation functions. The proposed approach integrates fuzzy logic operations, time-delay compensation, and non-smooth analysis techniques to establish robust synchronization criteria. Theoretical analyses verify that under the proposed control scheme, the synchronization error converges to zero within a prespecified time interval, independent of initial states.

1.3. Key innovations

The principal contributions and novel aspects of this work are manifested through the following key elements:

(1) An in-depth investigation is conducted on fuzzy Cohen-Grossberg neural networks incorporating discontinuous activation functions and time-varying delays, thereby extending previous continuous results reported in [3, 20–22] to the discontinuous scenario. It is particularly noteworthy that various existing delayed Cohen-Grossberg drive-response systems and fuzzy cellular drive-response models can be regarded as special cases of our proposed framework, as demonstrated in [4].
(2) Given the superior practical applicability of predefined-time synchronization compared to

asymptotic synchronization, the present research is dedicated to addressing the predefined-time synchronization control challenge for the developed model by establishing novel predefined-time stability theorems for discontinuous systems, which exhibit significant differences from and improvements upon existing results, while also providing a refined estimation of the settling time (ST) that demonstrates higher precision compared to previous estimates.

(3) This study develops an adaptive control scheme to solve the predefined-time synchronization issue in fuzzy Cohen-Grossberg neural networks. A distinctive feature of the proposed controller lies in its capability to directly adjust synchronization duration through predefined control parameters.

The organizational framework of this paper is presented below. Section 2 provides the system formulation and fundamental preliminaries. Section 3 introduces two control design approaches aimed at achieving predefined-time and fixed-time synchronization. Section 4 demonstrates the effectiveness of the proposed methods through numerical examples. Lastly, Section 5 provides the conclusion of the study.

2. System description and preliminaries

2.1. System description

This paper focuses on delayed FCGNNs that incorporate piecewise continuous activation functions, described as follows:

$$\begin{aligned}\dot{\mathcal{X}}_i(\mathfrak{c}) =& \urcorner d_i(\mathcal{X}_i(\mathfrak{c}))\Big[-\tau_i(\mathfrak{c},\mathcal{X}_i(\mathfrak{c})) + \bigwedge_{j=1}^{n} \alpha_{ij}(\mathfrak{c})\ \intercal_j\left(\mathcal{X}_j(\mathfrak{c}-\varrho_j(\mathfrak{c})-\vartheta_j(\mathfrak{c}))\right) + \sum_{j=1}^{n} a_{ij}(\mathfrak{c})\ \intercal_j\left(\mathcal{X}_j(\mathfrak{c})\right)\\ &+ \sum_{j=1}^{n} b_{ij}\nu_j + \bigvee_{j=1}^{n} g_{ij}(\mathfrak{c})\ \intercal_j\left(\mathcal{X}_j(\mathfrak{c}-\varrho_j(\mathfrak{c})-\vartheta_j(\mathfrak{c}))\right)\\ &+ \bigwedge_{j=1}^{n} T_{ij}\nu_j + \bigvee_{j=1}^{n} S_{ij}\nu_j + I_i(\mathfrak{c})\Big] \quad i=1,2,...,n.\end{aligned} \tag{2.1}$$

The system is initialized with: $\mathcal{X}_{i0}(\theta) = \phi_i(\theta), \quad \theta \in [-d, 0]$ where: $i, j = 1, 2, \ldots, n$ with $n \geq 2$ represents the number of neurons in the network. $\mathcal{X}_i(\mathfrak{c})$ describes the dynamic state of the i -th neuron at time t. $\urcorner d_i(\mathcal{X}_i(\mathfrak{c}))$ and $\tau_i(\mathcal{X}_i(\mathfrak{c}))$ correspond to the amplification and behavior functions, respectively. a_{ij} and b_{ij} are elements of feedback and feed-forward templates. The parameters α_{ij} and g_{ij} correspond to the fuzzy feedback MIN and MAX template components, respectively. The symbolic operators $\bigwedge$ and $\bigvee$ represent the fuzzy logical AND and OR operations, while T_{ij} and S_{ij} specify the fuzzy feed-forward MIN and MAX template elements.The variables ν_j and I_i denote the external input to the j-th neuron and the bias term of the i-th neuron, respectively. $\intercal_j$ is the neuronal activation function. $\vartheta_j(\mathfrak{c})$ and $\varrho_j(\mathfrak{c})$ are time-varying transmission and leakage delays satisfying: $0 \leq \vartheta_j(\mathfrak{c}) \leq \vartheta, \quad 0 \leq \varrho_j(\mathfrak{c}) \leq \varrho$ where $\vartheta = \max_{1\leq j\leq n} \sup_{\mathfrak{c}\in\mathbb{R}} |\vartheta_j(\mathfrak{c})|$ and $\varrho = \max_{1\leq j\leq n} \sup_{\mathfrak{c}\in\mathbb{R}} |\varrho_j(\mathfrak{c})|$ are finite bounds, with $d = \vartheta + \varrho$.

Remark 2.1. In contrast to the referenced study [23], our model demonstrates enhanced generality as it no longer imposes the restrictive assumptions of continuity and Lipschitz continuity on activation functions.

Considering the principle of drive-response synchronization, we designate system (2.1) as the driving component and formulate the corresponding response system as follows:

$$\begin{aligned}\dot{\mathcal{Y}}_i(\mathfrak{c}) =& \urcorner d_i(\mathcal{Y}_i(\mathfrak{c}))\Bigg[- \tau_i(\mathfrak{c}, \mathcal{Y}_i(\mathfrak{c})) + \bigwedge_{j=1}^{n} \alpha_{ij}(\mathfrak{c})\ \mathsf{T}_j\left(\mathcal{Y}_j(\mathfrak{c} - \varrho_j(\mathfrak{c}) - \vartheta_j(\mathfrak{c}))\right) + \sum_{j=1}^{n} a_{ij}(\mathfrak{c})\ \mathsf{T}_j\left(\mathcal{Y}_j(\mathfrak{c})\right) \\ &+ \sum_{j=1}^{n} b_{ij}\nu_j + \bigvee_{j=1}^{n} g_{ij}(\mathfrak{c})\ \mathsf{T}_j\left(\mathcal{Y}_j(\mathfrak{c} - \varrho_j(\mathfrak{c}) - \vartheta_j(\mathfrak{c}))\right) \\ &+ \bigwedge_{j=1}^{n} T_{ij}\nu_j + \bigvee_{j=1}^{n} S_{ij}\nu_j + I_i(\mathfrak{c})\Bigg] + u_i(\mathfrak{c}), \quad i = 1, 2, ..., n,\end{aligned} \tag{2.2}$$

with initial conditions, $\mathcal{Y}_{i0}(\theta) = \varphi_i(\theta), \theta \in [-d, 0]$, and $u_i(\mathfrak{c})$ is the control input that will be designed later.

The present study requires the following fundamental assumptions:

A1) For every index i (where $i = 1, 2, \ldots, n$), the function $\mathsf{T}_i\colon \mathbb{R} \to \mathbb{R}$ exhibits piecewise continuity. Specifically, T_i remains continuous across its domain except at a countable collection of points $\{\rho_k^i\}$. At each such point ρ_k^i, the righthand limit $\mathsf{T}_i^+(\rho_k^i)$ and the left-hand limit $\mathsf{T}_i^-(\rho_k^i)$ both exist and are finite. Furthermore, within any bounded subinterval of $\mathbb{R}$, the number of discontinuities of T_i is guaranteed to be finite.

A2) For each index i in the set $1, 2, ..., n$, one can define nonnegative coefficients $\mathcal{A}_i$ and $\mathcal{B}_i$ such that

$$\sup_{\gamma_i \in \overline{\text{co}}[\mathsf{T}_i(\mathcal{X}_i)], \eta_i \in \overline{\text{co}}[\mathsf{T}_i(\mathcal{Y}_i)]} |\gamma_i - \eta_i| \leq \mathcal{A}_i|\mathcal{X}_i - \mathcal{Y}_i| + \mathcal{B}_i, \forall F_i \quad , \mathcal{Y}_i \in \mathcal{R},$$

where

$$\begin{aligned}\overline{\text{co}}[\mathsf{T}_i(\mathcal{X}_i)] &= \left[\min\left\{\mathsf{T}_i^-(\mathcal{X}_i), \mathsf{T}_i^+(\mathcal{X}_i)\right\}, \max\left\{\mathsf{T}_i^-(\mathcal{X}_i), \mathsf{T}_i^+(\mathcal{X}_i)\right\}\right], \\ \overline{\text{co}}[\mathsf{T}_i(\mathcal{Y}_i)] &= \left[\min\left\{\mathsf{T}_i^-(\mathcal{Y}_i), \mathsf{T}_i^+(\mathcal{Y}_i)\right\}, \max\left\{\mathsf{T}_i^-(\mathcal{Y}_i), \mathsf{T}_i^+(\mathcal{Y}_i)\right\}\right].\end{aligned}$$

Furthermore, assuming the continuity of T_i at the point $\mathcal{X}_i$, the closed convex hull of $\mathsf{T}_i(\mathcal{X}_i)$ reduces to the singleton set $\{\mathsf{T}_i(\mathcal{X}_i)\}$.

A3) The function $\urcorner d_i(\mathcal{X})$ exhibits continuity and boundedness. Additionally, one can define two strictly positive constants, $\underline{d}_i$ and $\breve{d}_i$, satisfying the inequality:

$$0 < \underline{d}_i \leq \urcorner d_i(\mathcal{X}) \leq \breve{d}_i, \quad for \quad i = 1, 2, ..., n, \mathcal{X} \in \mathcal{R}.$$

A4) Given any $\mathcal{X} \in \mathcal{R}$, the function $\tau_i(\cdot, \mathcal{X})$ remains continuous.This function satisfies $\tau_i(\mathfrak{c}, 0) = 0$ for all $\mathfrak{c}$, and we can find a positive continuous function $\Lambda_i(\mathfrak{c}) > 0$ fulfilling the condition that

$$\frac{\tau_i(\mathfrak{c}, \mathcal{X}) - \tau_i(\mathfrak{c}, \mathcal{Y})}{\mathcal{X} - \mathcal{Y}} \geq \Lambda_i(\mathfrak{c}), \quad \mathcal{X}, \mathcal{Y} \in \mathcal{R},\ \mathcal{X} \neq \mathcal{Y}.$$

As implied by assumption (A3), we have $1/\urcorner d_i(\mathcal{X})$ is positive and continuous for all $\mathcal{X} \in \mathcal{R}$. Consider the transformation function $1/\hbar_i(\mathcal{X})$ defined to satisfy the differential equation:

$$\frac{d}{d\mathcal{X}}\hbar_i(\mathcal{X}) = \frac{1}{\urcorner d_i(\mathcal{X})}, \quad \text{with initial condition} \quad \hbar_i(0) = 0.$$

This construction ensures that $1/\hbar_i(\mathcal{X})$ is strictly monotone increasing in $\mathcal{X}$. Furthermore, the differentiability of the inverse function $\hbar_i^{-1}$ implies the relation: $\frac{d}{du}\hbar_i^{-1}(u) =^{\neg} d_i(u)$. We give the definition

$$z_i(\mathfrak{c}) = \hbar_i(\mathcal{X}_i(\mathfrak{c})),\ w_i(\mathfrak{c}) = \hbar_i(\mathcal{Y}_i(\mathfrak{c})),$$

and it can be directly obtained that

$$\mathcal{X}_i(\mathfrak{c}) = \hbar_i^{-1}(z_i(\mathfrak{c})), \quad \mathcal{Y}_i(\mathfrak{c}) = \hbar_i^{-1}(w_i(\mathfrak{c})),$$

and

$$\begin{cases} \dot{z}_i(\mathfrak{c}) = \dot{\mathfrak{c}}_i(\mathcal{X}_i(\mathfrak{c}))\dot{\mathcal{X}}_i(\mathfrak{c}) = \dfrac{\dot{\mathcal{X}}_i(\mathfrak{c})}{\neg d_i(\mathcal{X}_i(\mathfrak{c}))}, \\ \dot{w}_i(\mathfrak{c}) = \dot{\hbar}_i(\mathcal{Y}_i(\mathfrak{c}))\dot{\mathcal{Y}}_i(\mathfrak{c}) = \dfrac{\dot{\mathcal{Y}}_i(\mathfrak{c})}{\neg d_i(\mathcal{Y}_i(\mathfrak{c}))}. \end{cases}$$

By applying the aforementioned variable transformations to the original drive-response systems (2.1) and (2.2), we obtain the following expressions respectively:

$$\dot{z}_i(\mathfrak{c}) = \begin{cases} -\tau_i(\tau, \hbar_i^{-1}(z_i(\mathfrak{c}))) + \bigwedge_{j=1}^{n} \alpha_{ij}(\mathfrak{c}) \intercal_j (\hbar_j^{-1}(z_j(\mathfrak{c} - \varrho_j(\mathfrak{c}) - \vartheta_j(\mathfrak{c})))) \\ \quad + \sum_{j=1}^{n} a_{ij}(\mathfrak{c}) \intercal_j (\hbar_j^{-1}(z_j(\mathfrak{c}))) + \sum_{j=1}^{n} b_{ij}\nu_j + \bigwedge_{j=1}^{n} T_{ij}\nu_j \\ \quad + \bigvee_{j=1}^{n} g_{ij}(\mathfrak{c}) \intercal_j (\hbar_j^{-1}(z_j(\mathfrak{c} - \varrho_j(\mathfrak{c}) - \vartheta_j(\mathfrak{c})))) + \bigvee_{j=1}^{n} S_{ij}\nu_j + I_i(\mathfrak{c}), \\ z_{i0}(\theta) = \hbar_i(\phi_i(\theta)), \quad \theta \in [-d, 0], \quad i = 1, 2, \ldots, n, \end{cases} \tag{2.3}$$

$$\dot{w}_i(\mathfrak{c}) = \begin{cases} -\tau_i(\mathfrak{c}, \hbar_i^{-1}(w_i(\mathfrak{c}))) + \bigwedge_{j=1}^{n} \alpha_{ij}(\mathfrak{c}) \intercal_j (\hbar_j^{-1}(w_j(\mathfrak{c} - \varrho_j(\mathfrak{c}) - \vartheta_j(\mathfrak{c})))) \\ \quad + \sum_{j=1}^{n} a_{ij}(\mathfrak{c}) \intercal_j (\hbar_j^{-1}(w_j(\mathfrak{c}))) + \sum_{j=1}^{n} b_{ij}\nu_j + \bigwedge_{j=1}^{n} T_{ij}\nu_j \\ \quad + \bigvee_{j=1}^{n} g_{ij}(\mathfrak{c}) \intercal_j (\hbar_j^{-1}(w_j(\mathfrak{c} - \varrho_j(\mathfrak{c}) - \vartheta_j(\mathfrak{c})))) + \bigvee_{j=1}^{n} S_{ij}\nu_j + I_i(\mathfrak{c}) \\ \quad + \frac{u_i(\mathfrak{c})}{d_i(\hbar_i^{-1}(\text{Œ}_i(\mathfrak{c})))}, \\ \text{Œ}_{i0}(\theta) = \hbar_i(\varphi_i(\theta)), \quad \theta \in [-d, 0], \quad i = 1, 2, \ldots, n. \end{cases} \tag{2.4}$$

Consequently, the synchronization objective for systems (2.1) and (2.2) can be simplified to achieving synchronization between the transformed systems (2.3) and (2.4).

2.2. Fundamental concepts

The solution concept for discontinuous systems (2.3) and (2.4) will be established through Filippov's solution theory.

$z(\mathfrak{c}) = (z_1(\mathfrak{c}), z_2(\mathfrak{c}), ..., z_n(\mathfrak{c}))^\top$ and $w(\mathfrak{c}) = (w_1(\mathfrak{c}), w_2(\mathfrak{c}), ..., w_n(\mathfrak{c}))^\top$ as the vector-valued functions are considered, which represent solutions to the initial value problems (2.3) and (2.4) defined over the interval $[0, T)$, with $T \in (0, +\infty]$, For these solutions to be valid, each component $z_i(\mathfrak{c})$ and $w_i(\mathfrak{c})$ (where $i = 1, 2, ..., n$)must maintain absolute continuity on all compact subintervals within $[0, T)$ while

simultaneously satisfying the subsequent inclusion condition:

$$\begin{aligned}\dot{z}_i(\mathfrak{c}) \in & -\tau_i(\mathfrak{c}, \hbar_i^{-1}(z_i(\mathfrak{c}))) + \bigwedge_{j=1}^{n} \alpha_{ij}(\mathfrak{c})\overline{co}\Big[\ \mathsf{T}_j\left(\hbar_j^{-1}(z_j(\mathfrak{c}-\varrho_j(\mathfrak{c})-\vartheta_j(\mathfrak{c})))\right)\Big] \\ & + \sum_{j=1}^{n} a_{ij}(\mathfrak{c})\overline{co}[\mathsf{T}_j(\hbar_j^{-1}(z_j(\mathfrak{c})))] + \bigvee_{j=1}^{n} g_{ij}(\mathfrak{c})\overline{co}\Big[\ \mathsf{T}_j\left(\hbar_j^{-1}(z_j(\mathfrak{c}-\varrho_j(\mathfrak{c})-\vartheta_j(\mathfrak{c})))\right)\Big] \\ & + \sum_{j=1}^{n} b_{ij}\nu_j + \bigwedge_{j=1}^{n} T_{ij}\nu_j + \bigvee_{j=1}^{n} S_{ij}\nu_j + I_i(\mathfrak{c}), \text{ for } a.e.\ \mathfrak{c} \in [0,d),\ i = 1,2,...,n,\end{aligned}$$

and

$$\begin{aligned}\dot{w}_i(\mathfrak{c}) \in & -\ \tau_i(\mathfrak{c}, \hbar_i^{-1}(w_i(\mathfrak{c}))) + \bigwedge_{j=1}^{n} \alpha_{ij}(\mathfrak{c})\overline{co}\Big[\ \mathsf{T}_j\left(\hbar_j^{-1}(w_j(\mathfrak{c}-\varrho_j(\mathfrak{c})-\vartheta_j(\mathfrak{c})))\right)\Big] \\ & + \sum_{j=1}^{n} a_{ij}(\mathfrak{c})\overline{co}[\mathsf{T}_j(\hbar_j^{-1}(w_j(\mathfrak{c})))] + \sum_{j=1}^{n} b_{ij}\nu_j + \bigvee_{j=1}^{n} g_{ij}(\mathfrak{c})\overline{co}\Big[\ \mathsf{T}_j\left(\hbar_j^{-1}(w_j(\mathfrak{c}-\varrho_j(\mathfrak{c})-\vartheta_j(\mathfrak{c})))\right)\Big] \\ & + \bigwedge_{j=1}^{n} T_{ij}\nu_j + \bigvee_{j=1}^{n} S_{ij}\nu_j + I_i(\mathfrak{c}) + \frac{u_i(\mathfrak{c})}{\urcorner d_i(\hbar_i^{-1}(w_j(\mathfrak{c}))},\ \text{ for } a.e.\ \mathfrak{c} \in [0,d),\ i = 1,2,...,n.\end{aligned}$$

It follows directly that for $i = 1, 2, ..., n$, the corresponding set-valued mappings take the form:

$$\begin{aligned}\dot{z}_i(\mathfrak{c}) \hookrightarrow & -\tau_i(\mathfrak{c}, \hbar_i^{-1}(z_i(\mathfrak{c}))) + \bigwedge_{j=1}^{n} \alpha_{ij}(\mathfrak{c})\overline{co}\Big[\ \mathsf{T}_j\left(\hbar_j^{-1}(z_j(\mathfrak{c}-\varrho_j(\mathfrak{c})-\vartheta_j(\mathfrak{c})))\right)\Big] \\ & + \sum_{j=1}^{n} a_{ij}(\mathfrak{c})\overline{co}[\mathsf{T}_j(\hbar_j^{-1}(z_j(\mathfrak{c})))] + \sum_{j=1}^{n} b_{ij}\nu_j + \bigwedge_{j=1}^{n} T_{ij}\nu_j + \bigvee_{j=1}^{n} S_{ij}\nu_j + I_i(\mathfrak{c}) \\ & + \bigvee_{j=1}^{n} g_{ij}(\mathfrak{c})\overline{co}\Big[\ \mathsf{T}_j\left(\hbar_j^{-1}(z_j(\mathfrak{c}-\varrho_j(\mathfrak{c})-\vartheta_j(\mathfrak{c})))\right)\Big],\end{aligned}$$

and

$$\begin{aligned}\dot{w}_i(\mathfrak{c}) \hookrightarrow & -\tau_i(\mathfrak{c}, \hbar_i^{-1}(w_i(\mathfrak{c}))) + \bigwedge_{j=1}^{n} \alpha_{ij}(\mathfrak{c})\overline{co}\Big[\ \mathsf{T}_j\left(\hbar_j^{-1}(w_j(\mathfrak{c}-\varrho_j(\mathfrak{c})-\vartheta_j(\mathfrak{c})))\right)\Big] \\ & + \sum_{j=1}^{n} a_{ij}(\mathfrak{c})\overline{co}[\mathsf{T}_j(\hbar_j^{-1}(w_j(\mathfrak{c})))] + \sum_{j=1}^{n} b_{ij}\nu_j + \bigwedge_{j=1}^{n} T_{ij}\nu_j + \bigvee_{j=1}^{n} S_{ij}\nu_j + I_i(\mathfrak{c}) \\ & + \bigvee_{j=1}^{n} g_{ij}(\mathfrak{c})\overline{co}\Big[\ \mathsf{T}_j\left(\hbar_j^{-1}(w_j(\mathfrak{c}-\varrho_j(\mathfrak{c})-\vartheta_j(\mathfrak{c})))\right)\Big] + \frac{u_i(\mathfrak{c})}{\urcorner d_i(\hbar_i^{-1}(w_i(\mathfrak{c})))}.\end{aligned}$$

These set-valued mappings possess nonempty, compact, and convex values, ensuring their upper semicontinuity and measurability properties. Applying the measurable selection theorem to the solutions $z_i(\mathfrak{c})$ and $w_i(\mathfrak{c})$ of systems (2.3) and (2.4), we can establish the existence of measurable vector functions $\gamma = (\gamma_1, \gamma_2, ..., \gamma_n)^\top : [-d, T) \to \mathcal{R}^n$ and $\eta = (\eta_1, \eta_2, ..., \eta_n)^\top : [-d, T) \to \mathcal{R}^n$. These functions

satisfy the inclusion relations $\gamma_j(\mathfrak{c}) \in \overline{co}[\ \mathsf{T}_j\ (\hbar_j^{-1}(z_j(\mathfrak{c})))]$ and $\eta_j(\mathfrak{c}) \in \overline{co}[\ \mathsf{T}_j\ (\hbar_j^{-1}(w_j(\mathfrak{c})))]$ for almost every $\mathfrak{c} \in [-d, T)$.

$$\begin{aligned}\dot{z}_i(\mathfrak{c}) =& -\tau_i(\mathfrak{c}, \hbar_i^{-1}(z_i(\mathfrak{c}))) + \sum_{j=1}^{n} a_{ij}(\mathfrak{c})\gamma_j(\mathfrak{c}) + \sum_{j=1}^{n} b_{ij}\nu_j + \bigwedge_{j=1}^{n} T_{ij}\nu_j \\ &+ \bigwedge_{j=1}^{n} \alpha_{ij}(\mathfrak{c})\gamma_j(\mathfrak{c} - \varrho_j(\mathfrak{c}) - \vartheta_j(\mathfrak{c})) + \bigvee_{j=1}^{n} g_{ij}(\mathfrak{c})\gamma_j(\mathfrak{c} - \varrho_j(\mathfrak{c}) - \vartheta_j(\mathfrak{c})) \\ &+ \bigvee_{j=1}^{n} S_{ij}\nu_j + I_i(\mathfrak{c}),\ \text{for } a.e.\ \mathfrak{c} \geq 0,\ i = 1, 2, ..., n,\end{aligned} \tag{2.5}$$

and

$$\begin{aligned}\dot{w}_i(\mathfrak{c} =& -\tau_i(\mathfrak{c}, \hbar_i^{-1}(w_i(\mathfrak{c}))) + \sum_{j=1}^{n} a_{ij}(\mathfrak{c})\eta_j(\mathfrak{c}) + \sum_{j=1}^{n} b_{ij}\nu_j + \bigwedge_{j=1}^{n} T_{ij}\nu_j \\ &+ \bigwedge_{j=1}^{n} \alpha_{ij}(\mathfrak{c})\eta_j(\mathfrak{c} - \varrho_j(\mathfrak{c}) - \vartheta_j(\mathfrak{c})) + \bigvee_{j=1}^{n} g_{ij}(\mathfrak{c})\eta_j(\mathfrak{c} - \varrho_j(\mathfrak{c}) - \vartheta_j(\mathfrak{c})) \\ &+ \bigvee_{j=1}^{n} S_{ij}\nu_j + I_i(\mathfrak{c}) + \frac{u_i(\mathfrak{c})}{\urcorner d_i(\hbar_i^{-1}(w_i(\mathfrak{c})))},\ \text{for } a.e.\ \mathfrak{c} \geq 0,\ i = 1, 2, ..., n.\end{aligned} \tag{2.6}$$

Let the error variable be given by

$$e_i(\mathfrak{c}) = w_i(\mathfrak{c}) - z_i(\mathfrak{c}).$$

Then, combining Eqs (2.5) and (2.6) yields the error dynamic system:

$$\begin{aligned}\dot{e}_i(\mathfrak{c}) =& -\ [\tau_i(\mathfrak{c}, \hbar_i^{-1}(w_i(\mathfrak{c}))) - \tau_i(\mathfrak{c}, \hbar_i^{-1}(z_i(\mathfrak{c})))] + \sum_{j=1}^{n} a_{ij}(\mathfrak{c})[\eta_j(\mathfrak{c}) - \gamma_j(\mathfrak{c})] \\ &+ \bigwedge_{j=1}^{n} \alpha_{ij}(\mathfrak{c})[\eta_j(\mathfrak{c} - \varrho_j(\mathfrak{c}) - \vartheta_j(\mathfrak{c})) - \gamma_j(\mathfrak{c} - \varrho_j(\mathfrak{c}) - \vartheta_j(\mathfrak{c}))] \\ &+ \bigvee_{j=1}^{n} g_{ij}(\mathfrak{c})[\eta_j(\mathfrak{c} - \varrho_j(\mathfrak{c}) - \vartheta_j(\mathfrak{c})) - \gamma_j(\mathfrak{c} - \varrho_j(\mathfrak{c}) - \vartheta_j(\mathfrak{c}))] \\ &+ \frac{u_i(\mathfrak{c})}{\urcorner d_i(\hbar_i^{-1}(w_i(\mathfrak{c})))},\end{aligned} \tag{2.7}$$

with initial conditions

$$e_{i0}(\theta) = \hbar_i(\varphi_i(\theta)) - \hbar_i(\phi_i(\theta)),\ \theta \in [-d, 0].$$

For convenience, let $e_0(\theta) = (e_{10}(\theta), e_{20}(\theta), ..., e_{n0}(\theta))^{\top}, \theta \in [-d, 0]$.

Definition 2.1. (Predefined-time stability [24])

For vector ρ and a predefined-time constant $T_c := T_c(\rho) > 0$, the origin of system (2.1) is noted as (i) Globally weakly predefined-time stable for system (2.1) if it is fixed-time stable and the settling-time function $T : \mathbb{R}^n \to \mathbb{R}$ is such that $T(F_0) \leqslant T_c, \forall F_0 \in \mathbb{R}^n$. ii) Globally strongly predefined-time

stable for system (2.1) if it is fixed-time stable and the settling-time function $T : \mathbb{R}^n \to \mathbb{R}$ is such that $\sup_{x_0 \in \mathbb{R}^n} T(F_0) = T_c$.

Definition 2.2. If the error system (2.7) achieves predefined-time stability according to Definition 2.1, then the drive system (2.5) and the response system (2.6) will realize predefined-time synchronization.

Lemma 2.1. (See [25, 26]) Suppose $\mathcal{X}$ and $\mathcal{Y}$ are two states of system (2.1). Then, the following inequalities hold:

$$\left| \bigwedge_{j=1}^{n} \alpha_{ij} \, \mathsf{T}_j(\mathcal{X}_j) - \bigwedge_{j=1}^{n} \alpha_{ij} \, \mathsf{T}_j(\mathcal{Y}_j) \right| \leq \sum_{j=1}^{n} |\alpha_{ij}| \left| \mathsf{T}_j(\mathcal{X}_j) - \mathsf{T}_j(\mathcal{Y}_j) \right|, \tag{2.8}$$

$$\left| \bigvee_{j=1}^{n} g_{ij} \, \mathsf{T}_j(\mathcal{X}_j) - \bigvee_{j=1}^{n} g_{ij} \, \mathsf{T}_j(\mathcal{Y}_j) \right| \leq \sum_{j=1}^{n} |g_{ij}| \left| \mathsf{T}_j(\mathcal{X}_j) - \mathsf{T}_j(\mathcal{Y}_j) \right|. \tag{2.9}$$

Lemma 2.2. (See [27]) Let $\mathcal{X}_1, \mathcal{X}_2, \ldots, \mathcal{X}_n \geq 0$, $0 < p \leq 1$, $q > 1$. Then:

$$\sum_{i=1}^{n} \mathcal{X}_i^p \geq \left(\sum_{i=1}^{n} \mathcal{X}_i \right)^p, \quad \sum_{i=1}^{n} \mathcal{X}_i^q \geq n^{1-q} \left(\sum_{i=1}^{n} \mathcal{X}_i \right)^q.$$

Lemma 2.3. (see [28]) Consider the system $\dot{F} = \mathsf{T}(F)$. If there exists a continuous function $V(F)$, scalars $\upsilon > 0$, $\alpha > 0$, $0 < \xi < 1$, and $m > 0$ such that

$$\dot{V}(F) \leq -\upsilon V(F) - \alpha V^{\xi}(F) + m,$$

then the trajectory of system $\dot{F} = \mathsf{T}(F)$ is practical fixed-time stable. The residual set of the solution is given by

$$\left\{ F \,\middle|\, \limsup_{\mathfrak{c} \to \infty} V(F) \leq \min \left\{ \frac{m}{(1-\theta)\upsilon}, \left(\frac{m}{(1-\theta)\alpha} \right)^{\frac{1}{\xi}} \right\} \right\}$$

for some $0 < \theta < 1$, where θ_0 satisfies $0 < \theta_0 < 1$. The setting time is bounded as

$$T_r \leq \max\{\mathfrak{c}_0 + \frac{1}{\theta_0 \upsilon (1-\xi)} \ln \frac{\theta_0 \upsilon V^{1-\xi}(\mathfrak{c}_0) + \alpha}{\alpha}, \mathfrak{c}_0 + \frac{1}{\upsilon(1-\xi)} \ln \frac{\upsilon V^{1-\xi}(\mathfrak{c}_0) + \theta_0 \alpha}{\theta_0 \alpha}\}. \tag{2.10}$$

Lemma 2.4. (See [29]) Suppose $V(\cdot) : \mathbb{R}^n \to \mathbb{R}_+ \cup \{0\}$ is a continuous, radially unbounded function and satisfies:

(1) $V(e(\mathfrak{c})) = 0 \Leftrightarrow e(\mathfrak{c}) = 0$.
(2) For any $e(\mathfrak{c}) \neq 0$, there exist constants $\alpha, \mathcal{G}, m > 0$, $0 < \xi < 1$, and $\eta > 1$ such that

$$\dot{V}(e(\mathfrak{c})) \leq -\alpha V^{\xi}(e(\mathfrak{c})) - g V^{\eta}(e(\mathfrak{c})) - m. \tag{2.11}$$

(3) If $e(\mathfrak{c}) = 0$, then $\dot{V}(e(\mathfrak{c})) \leq 0$.

Then the zero solution of system (2.7) is fixed-time stable, and the settling time satisfies

$$T_{\max_1} = \frac{(\alpha^{\frac{1}{\xi}} + m^{\frac{1}{\xi}})^{1-\xi} - m^{\frac{1-\xi}{\xi}}}{\alpha^{\frac{1}{\xi}}(1-\xi)} + \frac{2^{\eta-1} \left(g^{\frac{1}{\eta}} + m^{\frac{1}{\eta}} \right)^{1-\eta}}{g^{\frac{1}{\eta}}(\eta - 1)}. \tag{2.12}$$

Theorem 2.1. Consider the dynamical system described by (2.7), Suppose there exists a radially unbounded Lyapunov function candidate $V(e(\mathfrak{c})) : R \to R$, that is strictly positive definite, where T_c denotes a tunable parameter. The system is guaranteed to exhibit the desired behavior, provided the following criteria are satisfied:

(1) $V(e(\mathfrak{c})) = 0 \Leftrightarrow e(\mathfrak{c}) = 0$.
(2) For any $V(e(\mathfrak{c})) > 0$, there exist α, g, m, G_c, $T_c > 0$, $0 < \xi < 1$, $\eta > 1$, where $\upsilon < \min\{\alpha, g\}$ satisfying

$$D^+V(F(\mathfrak{c})) \leq \frac{G_c}{T_c}(-\alpha V^{\xi}(e(\mathfrak{c})) - gV^{\eta}(e(\mathfrak{c})) + \upsilon V(e(\mathfrak{c})) - m). \tag{2.13}$$

Then, within the predefined time $T_c = T_{\max_2}$, the origin of system (2.7) exhibits predefined - time stability.

$$T_{\max_2} = G_c = \frac{\left[(\alpha-\upsilon)^{\frac{1}{\xi}} + m^{\frac{1}{\xi}}\right]^{1-\xi} - m^{\frac{1-\xi}{\xi}}}{(\alpha-\upsilon)^{\frac{1}{\xi}}(1-\xi)} + \frac{2^{\eta-1}\left[(g-\upsilon)^{\frac{1}{\eta}} + m^{\frac{1}{\eta}}\right]^{1-\eta}}{(g-\upsilon)^{\frac{1}{\eta}}(\eta-1)}.$$

Proof. The function representing the settling time can be written as

$$T(e(0)) \leq \int_{V(e(0))}^{0} \frac{G_c}{T_c} \frac{1}{-\alpha u^{\xi} - gu^{\eta} + \upsilon u - m} du \leq \int_{0}^{V(e(0))} \frac{T_c}{G_c} \frac{1}{\alpha u^{\xi} + gu^{\eta} - \upsilon u + m} du.$$

About $\upsilon < \min\{\alpha, g\}$, two cases can be identified $0 < \upsilon < \min\{\alpha, g\}$, $\upsilon \leq 0$.
Case 1: where $0 < \upsilon < \min\{\alpha, g\}$.
Case 1.1: $0 < V(e(0)) \leq 1$, consequently, it follows that

$$\begin{aligned}
T(e(0)) &\leq \int_0^{V(e(0))} \frac{T_c}{G_c} \frac{1}{\alpha u^{\xi} + gu^{\eta} - \upsilon u + m} du \leq \int_0^1 \frac{T_c}{G_c} \frac{1}{\alpha u^{\xi} + gu^{\eta} - \upsilon u + m} du \\
&\leq \int_0^1 \frac{T_c}{G_c} \frac{1}{\alpha u^{\xi} + gu^{\eta} - \upsilon u^{\xi} + m} du = \int_0^1 \frac{T_c}{G_c} \frac{1}{(\alpha-\upsilon) u^{\xi} + gu^{\eta} + m} du \\
&\leq \int_0^1 \frac{T_c}{G_c} \frac{1}{(\alpha-\upsilon) u^{\xi} + m} du = \frac{T_c}{G_c} \int_0^1 \frac{1}{[(\alpha-\upsilon)^{1/\xi} u + m^{1/\xi}]^{\xi}} du \\
&= \frac{T_c}{G_c} \frac{\left[(\alpha-\upsilon)^{1/\xi} + m^{1/\xi}\right]^{1-\xi} - m^{(1-\xi)/\xi}}{(\alpha-\upsilon)^{1/\xi}(1-\xi)}.
\end{aligned}$$

Case 1.2: $V(e(0)) > 1$,consequently, it follows that

$$\begin{aligned}
T\,(e(0)) &\leq \int_0^{V(e(0))} \frac{T_c}{G_c} \frac{1}{\alpha u^{\xi} + gu^{n} - \upsilon u + m} du \\
&\leq \int_0^1 \frac{T_c}{G_c} \frac{1}{\alpha u^{\xi} + gu^{\eta} - \upsilon u + m} du + \int_1^{V(e(0))} \frac{T_c}{G_c} \frac{1}{\alpha u^{\xi} + gu^{\eta} - \upsilon u + m} du \\
&\leq \int_0^1 \frac{T_c}{G_c} \frac{1}{\alpha u^{\xi} - \upsilon u^{\xi} + m} du + \int_1^{+\infty} \frac{T_c}{G_c} \frac{1}{gu^{\eta} - \upsilon u^{\eta} + m} du.
\end{aligned}$$

Similarity, we have

$$
\begin{aligned}
T(e(0)) &\leq \int_0^1 \frac{T_c}{G_c}\frac{1}{(\alpha-\upsilon)u^{\xi}+m}du + \int_1^{+\infty}\frac{T_c}{G_c}\frac{1}{(g-\upsilon)u^{\eta}+m}du \\
&= \frac{T_c}{G_c}\frac{\left[(\alpha-\upsilon)^{\frac{1}{\xi}}+m^{\frac{1}{\xi}}\right]^{1-\xi}-m^{\frac{1-\xi}{\xi}}}{(\alpha-\upsilon)^{\frac{1}{\xi}}(1-\xi)} + \frac{T_c}{G_c}\frac{2^{\eta-1}\left[(g-\upsilon)^{\frac{1}{\eta}}+m^{\frac{1}{\eta}}\right]^{1-\eta}}{(g-\upsilon)^{\frac{1}{\eta}}(\eta-1)} \\
&= \frac{T_c}{G_c}\left[\frac{\left[(\alpha-\upsilon)^{\frac{1}{\xi}}+m^{\frac{1}{\xi}}\right]^{1-\xi}-m^{\frac{1-\xi}{\xi}}}{(\alpha-\upsilon)^{\frac{1}{\xi}}(1-\xi)} + \frac{2^{\eta-1}\left[(g-\upsilon)^{\frac{1}{\eta}}+m^{\frac{1}{\eta}}\right]^{1-\eta}}{(g-\upsilon)^{\frac{1}{\eta}}(\eta-1)}\right] \\
&\leq T_c.
\end{aligned}
$$

Case 2: where $\upsilon \leq 0$.

Case 2.1: $0 < V(e(0)) \leq 1$, thus, we arrive at

$$
\begin{aligned}
T(e(0)) &\leq \int_0^{V(e(0))}\frac{T_c}{G_c}\frac{du}{\alpha u^{\xi}+gu^{\eta}-\upsilon u+m} \leq \int_0^{V(e(0))}\frac{T_c}{G_c}\frac{1}{\alpha u^{\xi}+gu^{\eta}+m}du \\
&\leq \int_0^1 \frac{T_c}{G_c}\frac{1}{\alpha u^{\xi}+m}du.
\end{aligned}
$$

When this is combined with Lemma 2.2, the result is

$$
\begin{aligned}
T(e(0)) &\leq \int_0^1 \frac{1}{\alpha u^{\xi}+m}du \leq \int_0^1 \frac{T_c}{G_c}\frac{1}{(\alpha^{\frac{1}{\xi}}u+m^{\frac{1}{\xi}})^{\xi}}du \\
&= \frac{T_c}{G_c}\frac{\left(\alpha^{\frac{1}{\xi}}+m^{\frac{1}{\xi}}\right)^{1-\xi}-m^{\frac{1-\xi}{\xi}}}{\alpha^{\frac{1}{\xi}}(1-\xi)}.
\end{aligned}
$$

Case 2.2: $V(e(0)) > 1$, accordingly, we attain

$$
\begin{aligned}
T(e(0)) &\leq \int_0^{V(e(0))}\frac{T_c}{G_c}\frac{du}{\alpha u^{\xi}+gu^{\eta}-\upsilon u+m} \\
&\leq \int_0^1 \frac{T_c}{G_c}\frac{du}{\alpha u^{\xi}+gu^{\eta}+m} + \int_1^{V(e(0))}\frac{T_c}{G_c}\frac{du}{\alpha u^{\xi}+gu^{\eta}+m} \\
&\leq \int_0^1 \frac{T_c}{G_c}\frac{du}{\alpha u^{\xi}+m} + \int_1^{+\infty}\frac{T_c}{G_c}\frac{du}{gu^{\eta}+m}.
\end{aligned}
$$

By leveraging Lemma 2.2, we derive

$$
\begin{aligned}
T(e(0)) &\leq \int_0^1 \frac{T_c}{G_c}\frac{du}{\alpha u^{\xi}+m} + \int_1^{+\infty}\frac{T_c}{G_c}\frac{du}{gu^{\eta}+m} \\
&\leq \frac{T_c}{G_c}\frac{\left(\alpha^{\frac{1}{\xi}}+m^{\frac{1}{\xi}}\right)^{1-\xi}-m^{\frac{1-\xi}{\xi}}}{\alpha^{\frac{1}{\xi}}(1-\xi)} + \int_1^{+\infty}\frac{T_c}{G_c}\frac{du}{gu^{\eta}+m} \\
&\leq \frac{T_c}{G_c}\frac{\left(\alpha^{\frac{1}{\xi}}+m^{\frac{1}{\xi}}\right)^{1-\xi}-m^{\frac{1-\xi}{\xi}}}{\alpha^{\frac{1}{\xi}}(1-\xi)} + \frac{T_c}{G_c}\frac{2^{\eta-1}\left(g^{\frac{1}{\eta}}+m^{\frac{1}{\eta}}\right)^{1-\eta}}{g^{\frac{1}{\eta}}(\eta-1)}
\end{aligned}
$$

$$\leq \frac{T_c}{G_c}\left[\frac{\left(\alpha^{\frac{1}{\xi}}+m^{\frac{1}{\xi}}\right)^{1-\xi}-m^{\frac{1-\xi}{\xi}}}{\alpha^{\frac{1}{\xi}}(1-\xi)}+\frac{2^{\eta-1}\left(g^{\frac{1}{\eta}}+m^{\frac{1}{\eta}}\right)^{1-\eta}}{g^{\frac{1}{\eta}}(\eta-1)}\right]$$
$$\leq T_c.$$

It follows that when υ, the parameter T_c in Case 2 coincides with T_c in Case 1. Having satisfied all necessary conditions, we may now formulate our central theorem. □

Remark 2.2. The present work makes three key advances. First, Theorems 2.1 formulate previously undisclosed inequality conditions. Second, they develop genuinely novel fixed-time stability criteria for discontinuous function dynamical systems (DFDS), complete with settling time bounds involving our newly introduced parameters. Third, and most importantly, these results properly subsume those in [29, 30] as special cases, establishing their broader theoretical scope.

Theorem 2.2. If $m \geq \max\left\{(g-\upsilon)^{\eta/\xi}, m_0\right\}$, $\alpha > \upsilon$, $g > \rho$, $\xi \in (0,1), \eta > 1, \theta_0 \in (0,1)$, $\alpha > \upsilon, g > \upsilon$, $\xi \in (0,1)$, $\eta > 1$, $\theta_0 \in (0,1)$, we have $T_{\max_2} < T_r$.

Proof. We aim to prove the following inequality under the given conditions:

$$L_1 + L_2 < \max\{T_1, T_2\},$$

where:

$$L_1 = \frac{\left[(\alpha-\upsilon)^{\frac{1}{\xi}}+m^{\frac{1}{\xi}}\right]^{1-\xi}-m^{\frac{1-\xi}{\xi}}}{(\alpha-\upsilon)^{\frac{1}{\xi}}(1-\xi)}, \quad L_2 = \frac{2^{\eta-1}\left[(g-\upsilon)^{\frac{1}{\eta}}+m^{\frac{1}{\eta}}\right]^{1-\eta}}{(g-\upsilon)^{\frac{1}{\eta}}(\eta-1)},$$
$$T_1 = \mathfrak{c}_0 + \frac{1}{\theta_0\upsilon(1-\xi)}\ln\left(1+\frac{\theta_0\upsilon V^{1-\xi}(\mathfrak{c}_0)}{\alpha}\right), \quad T_2 = \mathfrak{c}_0 + \frac{1}{\upsilon(1-\xi)}\ln\left(1+\frac{\upsilon V^{1-\xi}(\mathfrak{c}_0)}{\theta_0\alpha}\right),$$

subject to the limit condition:

$$\lim_{\mathfrak{c}\to\infty} V(F(\mathfrak{c})) \leq \min\left\{\frac{m}{(1-\theta)\upsilon}, \left(\frac{m}{(1-\theta)\alpha}\right)^{\frac{1}{\xi}}\right\}.$$

Assumptions: $\alpha > \upsilon$, $g > \upsilon$ (to ensure positivity under roots), $\xi \in (0,1)$, $\eta > 1$ (to ensure exponents are well-defined), $m > 0$, $V(\mathfrak{c}_0) > 0$, $\theta_0 \in (0,1)$, $\upsilon > 0$.

(1) Bounding the left-hand side (LHS)

Let $L = L_1 + L_2$, and $x = (\alpha-\upsilon)^{\frac{1}{\xi}}$, $y = m^{\frac{1}{\xi}}$, $u = (g-\upsilon)^{\frac{1}{\eta}}$, $v = m^{\frac{1}{\eta}}$.

(a) Boundedness analysis of L_1:

$$L_1 = \frac{(x+y)^{1-\xi}-y^{1-\xi}}{x(1-\xi)}.$$

By the integral inequality:

$$(x+y)^{1-\xi}-y^{1-\xi} = (1-\xi)\int_y^{x+y}\tau^{-\xi}d\tau \leq (1-\xi)xy^{-\xi},$$

we obtain: $L_1 \leq y^{-\xi} = m^{-1}$.

(b) Boundedness analysis of L_2:

$$L_2 = \frac{2^{\eta-1}(u+v)^{1-\eta}}{u(\eta-1)}.$$

For $\eta > 1$ and $v \geq u$ (i.e., $m \geq (g-\upsilon)^{\eta/\xi}$):

$$(u+v)^{1-\eta} \leq v^{1-\eta},$$

thus:

$$L_2 \leq \frac{2^{\eta-1}v^{1-\eta}}{u(\eta-1)} = \frac{2^{\eta-1}m^{\frac{1-\eta}{\eta}}}{(g-\upsilon)^{\frac{1}{\eta}}(\eta-1)}.$$

(c) Combined bound for L:

$$L \leq m^{-1} + \frac{2^{\eta-1}m^{\frac{1-\eta}{\eta}}}{(g-\upsilon)^{\frac{1}{\eta}}(\eta-1)}.$$

(2) Analysis of the right-hand side (RHS). The RHS is $\max\{T_1, T_2\}$. We analyze both terms:
(a) Bound for $V(\mathfrak{c}_0)$: from the limit condition:

$$V(\mathfrak{c}_0) \leq \left(\frac{m}{(1-\theta)\alpha}\right)^{\frac{1}{\xi}} \implies V^{1-\xi}(\mathfrak{c}_0) \leq \left(\frac{m}{(1-\theta)\alpha}\right)^{\frac{1-\xi}{\xi}}.$$

(b) Asymptotic expansion of T_1 and T_2: For T_1:

$$T_1 \leq \mathfrak{c}_0 + \frac{1}{\theta_0\upsilon(1-\xi)}\ln\left(1 + \frac{\theta_0\rho}{\alpha}\left(\frac{m}{(1-\theta)\alpha}\right)^{\frac{1-\xi}{\xi}}\right).$$

For T_2:

$$T_2 \leq \mathfrak{c}_0 + \frac{1}{\rho(1-\xi)}\ln\left(1 + \frac{\upsilon}{\theta_0\alpha}\left(\frac{m}{(1-\theta)\alpha}\right)^{\frac{1-\xi}{\xi}}\right).$$

(c) Dominant terms for $m \to \infty$:

$$T_1 \sim \mathfrak{c}_0 + \frac{\ln m}{\theta_0\upsilon\xi}, \quad T_2 \sim \mathfrak{c}_0 + \frac{\ln m}{\upsilon\xi}.$$

Since $\theta_0 \in (0,1)$, T_2 dominates:

$$\max\{T_1, T_2\} = T_2 \sim \mathfrak{c}_0 + \frac{\ln m}{\upsilon\xi}.$$

(3) Verification of the inequality. We require:

$$L \leq m^{-1} + \frac{2^{\eta-1}m^{\frac{1-\eta}{\eta}}}{(g-\upsilon)^{\frac{1}{\eta}(\eta-1)}} < \mathfrak{c}_0 + \frac{\ln m}{\upsilon\xi}.$$

(a) Decay of L: $m^{-1} \to 0$ (exponential decay), $m^{\frac{1-\eta}{\eta}} \to 0$ (since $\eta > 1$). (b) Growth of T_2: $\frac{\ln m}{\upsilon\xi} \to +\infty$ (logarithmic growth). Thus, there exists $m_0 > 0$ such that for all $m \geq m_0$, the inequality holds. Under the stated conditions, for sufficiently large m,

$$L < T_2 = \max\{T_1, T_2\},$$

with the asymptotic behavior of T_2 dominated by $\frac{\ln m}{\upsilon\xi}$. This completes the proof. □

Remark 2.3. From Lemma 2.3 and Theorem 2.2, we observe that both provide estimates for the settling times STs. However, the theorem reveals that $T_{\max_2} < T_r$ when m is sufficiently large. This implies that: Theorem 2.1 imposes less restrictive conditions compared to Lemma 2.3. The control strategy derived from Theorem 2.2 offers superior performance characteristics, as evidenced by: Faster convergence (shorter settling times), broader applicability (valid for larger parameter ranges),and improved robustness (better tolerance to system variations).

3. Main results of synchronization

3.1. Synchronization within predefined time intervals achieved by a discontinuous state - feedback controller

Theorem 3.1. Based on A1-4 and controller (3.1), take into account a positive definite diagonal matrix function $Q(\mathfrak{c}) = diag(q_1(\mathfrak{c}), q_2(\mathfrak{c}), \cdots q_n(\mathfrak{c})) \in R^{n\times n}$ that complies with the inequality $\dot{Q}(\mathfrak{c}) \geq \varepsilon I_n$, where ε represents a positive constant. If

$$\frac{2}{\breve{d}_i}\lambda_1 k_{i1} \geq \sum_{j=1}^{n}[2\lambda_2 a_{ij}(\mathfrak{c})\ \mathcal{B}_j + 2\lambda_2\left|\alpha_{ij}(\mathfrak{c})\right|\mathcal{B}_j + 2\lambda_2\left|g_{ij}(\mathfrak{c})\right|\mathcal{B}_j],$$

$$\frac{2}{\breve{d}_i}\lambda_1 k_{i2} \geq \dot{q}_i(\mathfrak{c}) - 2\lambda_1\sum_{i=1}^{n}\Lambda_i(\mathfrak{c})\breve{d}_i + 2\lambda_2\underline{d_i}\mathcal{A}_j a_{ij}(\mathfrak{c}),$$

$$\frac{2}{\breve{d}_i}k_{i3} \geq \left|\alpha_{ij}(\mathfrak{c})\right| + \left|g_{ij}(\mathfrak{c})\right|,$$

$$G_c = \frac{\left(\alpha^{\frac{1}{\xi}} + m^{\frac{1}{\xi}}\right)^{1-\xi} - m^{\frac{1-\xi}{\xi}}}{\alpha^{\frac{1}{\xi}}(1-\xi)} + \frac{2^{\eta-1}\left(g^{\frac{1}{\eta}} + m^{\frac{1}{\eta}}\right)^{1-\eta}}{g^{\frac{1}{\xi}}(\eta-1)},$$

under such circumstances, systems (2.5) and (2.6) accomplish the predefined-time synchronization. This controller is:

$$\begin{aligned} u_i(\mathfrak{c}) =& -k_{i1}\text{sign}(e_i(\mathfrak{c}))) - k_{i2}\text{sign}(e_i(\mathfrak{c}))|e_i(\mathfrak{c})| - k_{i3}\text{sign}(e_i(\mathfrak{c}))|e_i(\mathfrak{c}-d)| \\ &+ \frac{G_c}{T_c}\Big(-\alpha\text{sign}(e_i(\mathfrak{c}))|e_i(\mathfrak{c})|^p - g\text{sign}(e_i(\mathfrak{c}))|e_i(\mathfrak{c})|^q + \upsilon e_i(\mathfrak{c}) - m\Big), \end{aligned} \tag{3.1}$$

where $k_{i1}, k_{i2}, k_{i3}, G_c, T_c, \alpha, g > 0, 0 < p < 1, q > 1, m > 0$, and $\breve{d}_i = max\{\breve{d}_i\}$, $\lambda_1 = inf_{\mathfrak{c}\geq 0}\{\lambda_{min}(Q(\mathfrak{c}))\}$, $\lambda_2 = \sup_{\mathfrak{c}\geq 0}\{\lambda_{\max}(Q(\mathfrak{c}))\}$, $d = \max\{\varrho + \vartheta\}$.

Proof. The subsequent Lyapunov function is formulated as:

$$V(t) = e^T(\mathfrak{c})Q(\mathfrak{c})e(\mathfrak{c}).$$

Upon computing the derivative of the function $V(\mathfrak{c})$, the following outcomes are obtained:

$$D^+V(\mathfrak{c}) = \sum_{i=1}^{n}\left[2q_i(\mathfrak{c})e_i(\mathfrak{c})\dot{e}_i(\mathfrak{c}) + \dot{q}_i(\mathfrak{c})e_i^2(\mathfrak{c})\right]$$

$$
\begin{aligned}
&= \sum_{i=1}^{n} 2q_i(\mathfrak{c})e_i(\mathfrak{c})\Big[-\Big(\tau_i(\mathfrak{c}, h_i^{-1}(w_i(\mathfrak{c}))) - \tau_i(\mathfrak{c}, h_i^{-1}(z_i(\mathfrak{c})))\Big)\Big] \\
&\quad + \sum_{i=1}^{n} 2q_i(\mathfrak{c})e_i(\mathfrak{c}) \sum_{j=1}^{n} a_{ij}(\mathfrak{c})\Big[\eta_j(\mathfrak{c}) - \gamma_j(\mathfrak{c})\Big] \\
&\quad + \sum_{i=1}^{n} 2q_i(\mathfrak{c})e_i(\mathfrak{c}) \bigwedge_{j=1}^{n} \alpha_{ij}(\mathfrak{c})\Big[\eta_j(\mathfrak{c} - \varrho_j(\mathfrak{c}) - \vartheta_j(\mathfrak{c})) - \gamma_j(\mathfrak{c} - \varrho_j(\mathfrak{c}) - \vartheta_j(\mathfrak{c}))\Big] \\
&\quad + \sum_{i=1}^{n} 2q_i(\mathfrak{c})e_i(\mathfrak{c}) \bigvee_{j=1}^{n} g_{ij}(\mathfrak{c})\Big[\eta_j(\mathfrak{c} - \varrho_j(\mathfrak{c}) - \vartheta_j(\mathfrak{c})) - \gamma_j(\mathfrak{c} - \varrho_j(\mathfrak{c}) - \vartheta_j(\mathfrak{c}))\Big] \\
&\quad + \sum_{i=1}^{n} 2q_i(\mathfrak{c})e_i(\mathfrak{c}) \frac{u_i(\mathfrak{c})}{\urcorner d_i(\hbar_i^{-1}(u_i(\mathfrak{c})))} \\
&\quad + \sum_{i=1}^{n} \dot{q}_i(\mathfrak{c})e_i^2(\mathfrak{c}).
\end{aligned} \tag{3.2}
$$

The existence of $\mu_1 \in \Big[\hbar_i^{-1}(w_i(\mathfrak{c})),\ \hbar_i^{-1}(z_i(\mathfrak{c}))\Big]$, $\mu_2 \in [w_i(\mathfrak{c}),\ z_i(\mathfrak{c})]$ can be established through an application of the mean value theorem under Assumptions 3 and 4.

$$
\begin{aligned}
&\sum_{i=1}^{n} 2q_i(\mathfrak{c})e_i(\mathfrak{c})\Big[-\Big(\tau_i(\mathfrak{c}, \hbar_i^{-1}(w_i(\mathfrak{c}))) - \tau_i(\mathfrak{c}, \hbar_i^{-1}(z_i(\mathfrak{c})))\Big)\Big] \\
&= -\sum_{i=1}^{n} 2q_i(\mathfrak{c})e_i(\mathfrak{c})\tau_i'(\mu_1)\Big(\hbar_i^{-1}(w_i(\mathfrak{c})) - \hbar_i^{-1}(z_i(\mathfrak{c}))\Big) \\
&= -\sum_{i=1}^{n} 2q_i(\mathfrak{c})e_i(\mathfrak{c})\Lambda_i(\mathfrak{c})(\hbar_i^{-1})'\mu_2(w_i(\mathfrak{c}) - z_i(\mathfrak{c})) \\
&\leq -2\lambda_1 \sum_{i=1}^{n} \underline{d}_i\Lambda_i(\mathfrak{c})|e_i(\mathfrak{c})|^2.
\end{aligned} \tag{3.3}
$$

According to Lemma 2.1, it can be concluded that

$$
\begin{aligned}
&\sum_{i=1}^{n} 2q_i(\mathfrak{c})e_i(\mathfrak{c}) \sum_{j=1}^{n} a_{ij}(\mathfrak{c})[\eta_j(\mathfrak{c}) - \gamma_j(\mathfrak{c})] \\
&\leq \sum_{i=1}^{n} 2q_i(\mathfrak{c})|e_i(\mathfrak{c})| \sum_{j=1}^{n} \Big|a_{ij}(\mathfrak{c})\Big[\mathcal{A}_j\Big(\hbar_j^{-1}(w_j(\mathfrak{c}))\Big) - \hbar_j^{-1}(z_j(\mathfrak{c}))\Big) + \mathcal{B}_j\Big]\Big| \\
&\leq \sum_{i=1}^{n} 2q_i(\mathfrak{c})|e_i(\mathfrak{c})| \sum_{j=1}^{n} \Big|a_{ij}(\mathfrak{c})\Big[\mathcal{A}_j(\hbar_j^{-1})'\mu_2(w_j(\mathfrak{c}) - z_j(\mathfrak{c}) + \mathcal{B}_j\Big]\Big| \\
&\leq \sum_{i=1}^{n} 2q_i(\mathfrak{c})|e_i(\mathfrak{c})| \sum_{j=1}^{n} \Big|a_{ij}(\mathfrak{c})[\mathcal{A}_j\breve{d}_i e_j(\mathfrak{c}) + \mathcal{B}_j]\Big| \\
&\leq \sum_{i=1}^{n} \sum_{j=1}^{n} 2\lambda_2\breve{d}_i\mathcal{A}_j|a_{ij}(\mathfrak{c})||e_i(\mathfrak{c})|^2 + \sum_{i=1}^{n} \sum_{j=1}^{n} 2\lambda_2\mathcal{B}_j|a_{ij}(\mathfrak{c})||e_i(\mathfrak{c})|.
\end{aligned} \tag{3.4}
$$

Utilizing Lemma 2.1 and Assumption 2, and applying the mean value theorem, we can demonstrate the existence of $\mu_3 \in \left[\hbar_i^{-1}(w_i(\mathfrak{c}-\varrho_j(\mathfrak{c})-\vartheta_j(\mathfrak{c}))), \hbar_i^{-1}(z_i(\mathfrak{c}-\varrho_j(\mathfrak{c})-\vartheta_j(\mathfrak{c})))\right]$ such that

$$
\begin{aligned}
&\sum_{i=1}^{n} 2q_i(\mathfrak{c})e_i(\mathfrak{c}) \bigwedge_{j=1}^{n} \alpha_{ij}(\mathfrak{c})\Big[\eta_j(\mathfrak{c}-\varrho_j(\mathfrak{c})-\vartheta_j(\mathfrak{c})) - \gamma_j(\mathfrak{c}-\varrho_j(\mathfrak{c})-\vartheta_j(\mathfrak{c}))\Big] \\
&\leq \sum_{i=1}^{n} 2q_i(\mathfrak{c})|e_i(\mathfrak{c})| \left| \bigwedge_{j=1}^{n} \alpha_{ij}(\mathfrak{c})\eta_j(\mathfrak{c}-\varrho_j(\mathfrak{c})-\vartheta_j(\mathfrak{c})) - \bigwedge_{j=1}^{n} \alpha_{ij}(\mathfrak{c})\gamma_j(\mathfrak{c}-\varrho_j(\mathfrak{c})-\vartheta_j(\mathfrak{c})) \right| \\
&\leq \sum_{i=1}^{n} 2q_i(\mathfrak{c})|e_i(\mathfrak{c})| \sum_{j=1}^{n} |\alpha_{ij}(\mathfrak{c})| \Big|\eta_j(\mathfrak{c}-\varrho_j(\mathfrak{c})-\vartheta_j(\mathfrak{c})) - \gamma_j(\mathfrak{c}-\varrho_j(\mathfrak{c})-\vartheta_j(\mathfrak{c}))\Big| \\
&\leq \sum_{i=1}^{n}\sum_{j=1}^{n} 2q_i(\mathfrak{c})|e_i(\mathfrak{c})||\alpha_{ij}(\mathfrak{c})| \Big|\mathcal{A}_j\Big(\hbar_j^{-1}(w_j(\mathfrak{c}-\varrho_j(\mathfrak{c})-\vartheta_j(\mathfrak{c})) - \hbar_j^{-1}(z_j(\mathfrak{c}-\varrho_j(\mathfrak{c})-\vartheta_j(\mathfrak{c}))\Big) + \mathcal{B}_j\Big| \qquad (3.5) \\
&\leq \sum_{i=1}^{n}\sum_{j=1}^{n} 2q_i(\mathfrak{c})|e_i(\mathfrak{c})||\alpha_{ij}(\mathfrak{c})| \Big|\mathcal{A}_j(\hbar_j^{-1})'\mu_3(w_j(\mathfrak{c}-\varrho_j(\mathfrak{c})-\vartheta_j(\mathfrak{c})) - z_j(\mathfrak{c}-\varrho_j(\mathfrak{c})-\vartheta_j(\mathfrak{c}))) + \mathcal{B}_j\Big| \\
&\leq \sum_{i=1}^{n}\sum_{j=1}^{n} 2q_i(\mathfrak{c})|e_i(\mathfrak{c})||\alpha_{ij}(\mathfrak{c})| \Big|\mathcal{A}_j\check{d}_j e_j(\mathfrak{c}-\varrho_j(\mathfrak{c})-\vartheta_j(\mathfrak{c})) + \mathcal{B}_j\Big| \\
&\leq \sum_{i=1}^{n}\sum_{j=1}^{n} 2\lambda_2|\alpha_{ij}(\mathfrak{c})|\mathcal{A}_j\check{d}_j|e_i(\mathfrak{c})||e_j(\mathfrak{c}-d)| + \sum_{i=1}^{n}\sum_{j=1}^{n} 2\lambda_2|\alpha_{ij}(\mathfrak{c})|\mathcal{B}_j|e_i(\mathfrak{c})|.
\end{aligned}
$$

Similarly, we have

$$
\begin{aligned}
&\sum_{i=1}^{n} 2q_i(\mathfrak{c})e_i(\mathfrak{c}) \bigvee_{j=1}^{n} g_{ij}(\mathfrak{c}) \left[\eta_j\left(\mathfrak{c}-\varrho_j(\mathfrak{c})-\vartheta_j(\mathfrak{c})\right) - \gamma_j\left(\mathfrak{c}-\varrho_j(\mathfrak{c})-\vartheta_j(\mathfrak{c})\right)\right] \\
&\leq \sum_{i=1}^{n} 2q_i(\mathfrak{c})\,|e_i(\mathfrak{c})| \left| \bigvee_{j=1}^{n} g_{ij}(\mathfrak{c})\eta_j\left(\mathfrak{c}-\varrho_j(\mathfrak{c})-\vartheta_j(\mathfrak{c})\right) - \bigvee_{j=1}^{n} g_{ij}(\mathfrak{c})\gamma_j\left(\mathfrak{c}-\varrho_j(\mathfrak{c})-\vartheta_j(\mathfrak{c})\right) \right| \\
&\leq \sum_{i=1}^{n}\sum_{j=1}^{n} 2q_i(\mathfrak{c})\,|e_i(\mathfrak{c})|\,\left|g_{ij}(\mathfrak{c})\right| \left|\eta_j\left(\mathfrak{c}-\varrho_j(\mathfrak{c})-\vartheta_j(\mathfrak{c})\right) - \gamma_j\left(\mathfrak{c}-\varrho_j(\mathfrak{c})-\vartheta_j(\mathfrak{c})\right)\right| \qquad (3.6) \\
&\leq \sum_{i=1}^{n}\sum_{j=1}^{n} 2q_i(\mathfrak{c})|e_i(\mathfrak{c})||g_{ij}(\mathfrak{c})| \left|\mathcal{A}_j\left(\hbar_j^{-1}\left(w_j(\mathfrak{c}-\varrho_j(\mathfrak{c})-\vartheta_j(\mathfrak{c}))\right) - \hbar_j^{-1}\left(z_j(\mathfrak{c}-\varrho_j(\mathfrak{c})-\vartheta_j(\mathfrak{c}))\right)\right) + \mathcal{B}_j\right| \\
&\leq \sum_{i=1}^{n}\sum_{j=1}^{n} 2q_i(\mathfrak{c})|e_i(\mathfrak{c})||g_{ij}(\mathfrak{c})| \left|\mathcal{A}_j(\hbar_j^{-1})'\mu_3(w_j(\mathfrak{c}-\varrho_j(\mathfrak{c})-\vartheta_j(\mathfrak{c})) - z_j(\mathfrak{c}-\varrho_j(\mathfrak{c})-\vartheta_j(\mathfrak{c}))) + \mathcal{B}_j\right| \qquad (3.7) \\
&\leq \sum_{i=1}^{n}\sum_{j=1}^{n} 2q_i(\mathfrak{c})|e_i(\mathfrak{c})||g_{ij}(\mathfrak{c})|\,\left|\mathcal{A}_j\check{d}_j e_i(\mathfrak{c}-\varrho_j(\mathfrak{c})-\vartheta_j(\mathfrak{c})) + \mathcal{B}_j\right| \\
&\leq \sum_{i=1}^{n}\sum_{j=1}^{n} 2\lambda_2\left|g_{ij}(\mathfrak{c})\right|\mathcal{A}_j\check{d}_j\,|e_i(\mathfrak{c})|\left|e_j\left(\mathfrak{c}-d\right)\right| + \sum_{i=1}^{n}\sum_{j=1}^{n} 2\lambda_2\left|g_{ij}(\mathfrak{c})\right|\mathcal{B}_j\,|e_i(\mathfrak{c})|\,.
\end{aligned}
$$

From Lemma 2.1, it follows that

$$
\begin{aligned}
&\sum_{i=1}^{n} 2q_i(\mathfrak{c})e_i(\mathfrak{c})\frac{1}{\urcorner d_i(\hbar_i^{-1}(w_i(\mathfrak{c})))}\\
&\times\Big[-k_{i1}\mathrm{sign}(e_i(\mathfrak{c}))-k_{i2}\mathrm{sign}(e_i(\mathfrak{c}))|e_i(\mathfrak{c})|-k_{i3}\mathrm{sign}(e_i(\mathfrak{c}))|e_i(\mathfrak{c}-\varrho_j(\mathfrak{c})-\vartheta_j(\mathfrak{c}))|\\
&+\frac{G_c}{T_c}\Big(-\alpha\mathrm{sign}(e_i(\mathfrak{c}))|e_i(\mathfrak{c})|^p-g\mathrm{sign}(e_i(\mathfrak{c}))|e_i(\mathfrak{c})|^q+\upsilon e_i(\mathfrak{c})-m\Big)\Big]\\
\leq&-\frac{2}{\breve{d}_i}\lambda_1k_{i1}|e_i(\mathfrak{c})|-\frac{2}{\breve{d}_i}\lambda_1k_{i2}|e_i(\mathfrak{c})|^2-\frac{2}{\breve{d}_i}\lambda_1k_{i3}|e_i(\mathfrak{c})||e_i(\mathfrak{c}-\varrho_j(\mathfrak{c})-\vartheta_j(\mathfrak{c}))|\\
&+\frac{G_c}{T_c}\Big(-\alpha\mathrm{sign}(e_i(\mathfrak{c}))|e_i(\mathfrak{c})|^p-g\mathrm{sign}(e_i(\mathfrak{c}))|e_i(\mathfrak{c})|^q+\upsilon e_i(\mathfrak{c})-m\Big)\Big]\\
\leq&-\frac{2}{\breve{d}_i}\lambda_1k_{i1}|e_i(\mathfrak{c})|-\frac{2}{\breve{d}_i}\lambda_1k_{i2}|e_i(\mathfrak{c})|^2-\frac{2}{\breve{d}_i}\lambda_1k_{i3}|e_i(\mathfrak{c})|\left|e_i(\mathfrak{c}-\varrho_j(\mathfrak{c})-\vartheta_j(\mathfrak{c}))\right|\\
&-\frac{2}{\breve{d}_i}\lambda_1\alpha\frac{G_c}{T_c}e_i(\mathfrak{c})|e_i(\mathfrak{c})|^p-\frac{2}{\breve{d}_i}\lambda_1\frac{G_c}{T_c}ge_i(\mathfrak{c})|e_i(\mathfrak{c})|^q+\frac{2}{\underline{d}_i}\upsilon\lambda_2\frac{G_c}{T_c}e_i^2(\mathfrak{c})-\frac{2}{\breve{d}_i}\lambda_1\frac{G_c}{T_c}me_i(\mathfrak{c})\\
\leq&-\frac{2}{\breve{d}_i}\lambda_1k_{i1}|e_i(\mathfrak{c})|-\frac{2}{\breve{d}_i}\lambda_1k_{i2}|e_i(\mathfrak{c})|^2-\frac{2}{\breve{d}_i}\lambda_1k_{i3}|e_i(\mathfrak{c})|\cdot|e_i(\mathfrak{c}-\varrho_j(\mathfrak{c})-\vartheta_j(\mathfrak{c}))| \qquad (3.8)\\
&+\frac{G_c}{T_c}\left[-\frac{2}{\breve{d}_i}\alpha\lambda_1\left(\sum_{i=1}^{n}e_i^2(\mathfrak{c})\right)^{\frac{p+1}{2}}-\frac{2}{\breve{d}_i}g\lambda_1n^{-q}\left(\sum_{i=1}^{n}e_i^2(\mathfrak{c})\right)^{\frac{q+1}{2}}+\frac{2}{\underline{d}_i}\upsilon\lambda_2e_i^2(\mathfrak{c})-\frac{2}{\breve{d}_i}\lambda_1me_i(\mathfrak{c})\right]\\
\leq&-\frac{2}{\breve{d}_i}\lambda_1k_{i1}|e_i(\mathfrak{c})|-\frac{2}{\breve{d}_i}\lambda_1k_{i2}|e_i(\mathfrak{c})|^2-\frac{2}{\breve{d}_i}\lambda_1k_{i3}|e_i(\mathfrak{c})||e_i(\mathfrak{c}-d)|\\
&+\frac{G_c}{T_c}\left[-\frac{2}{\breve{d}_i}\alpha\lambda_1\lambda_2^{\frac{p+1}{2}}V^{\frac{p+1}{2}}(\mathfrak{c})-\frac{2}{\breve{d}_i}g\lambda_1\lambda_2^{-\frac{p+1}{2}}n^{-q}V^{\frac{p+1}{2}}(\mathfrak{c})+\frac{2}{\breve{d}_i}\upsilon V(\mathfrak{c})-m\right].
\end{aligned}
$$

Combining formulas (3.2)–(3.8), hence, we conclude

$$
\begin{aligned}
D^+V(\mathfrak{c})\leq&\sum_{i=1}^{n}\sum_{j=1}^{n}2\lambda_2\breve{d}_i\mathcal{A}_j|a_{ij}(\mathfrak{c})||e_i(\mathfrak{c})|^2+\sum_{i=1}^{n}\sum_{j=1}^{n}2\lambda_2\mathcal{B}_j|a_{ij}(\mathfrak{c})||e_i(\mathfrak{c})|\\
&+\sum_{i=1}^{n}\sum_{j=1}^{n}2\lambda_2\breve{d}_i\mathcal{A}_j|a_{ij}(\mathfrak{c})||e_i(\mathfrak{c})|^2+\sum_{i=1}^{n}\sum_{j=1}^{n}2\lambda_2\mathcal{B}_j|a_{ij}(\mathfrak{c})||e_i(\mathfrak{c})|\\
&+\sum_{i=1}^{n}\sum_{j=1}^{n}2\lambda_2|\alpha_{ij}(\mathfrak{c})|\mathcal{A}_j\breve{d}_j|e_i(\mathfrak{c})||e_j(\mathfrak{c}-d)|+\sum_{i=1}^{n}\sum_{j=1}^{n}2\lambda_2|\alpha_{ij}(\mathfrak{c})|\mathcal{B}_j|e_i(\mathfrak{c})|.\\
&+\sum_{i=1}^{n}\sum_{j=1}^{n}2\lambda_2\left|g_{ij}(\mathfrak{c})\right|\mathcal{A}_j\breve{d}_j|e_i(\mathfrak{c})|\left|e_j(\mathfrak{c}-d)\right|+\sum_{i=1}^{n}\sum_{j=1}^{n}2\lambda_2\left|g_{ij}(\mathfrak{c})\right|\mathcal{B}_j|e_i(\mathfrak{c})|.\\
&+\frac{G_c}{T_c}\left[-\frac{2}{\breve{d}_i}\alpha\lambda_1\lambda_2^{\frac{p+1}{2}}V^{\frac{p+1}{2}}(\mathfrak{c})-\frac{2}{\breve{d}_i}g\lambda_1\lambda_2^{-\frac{p+1}{2}}n^{-q}V^{\frac{p+1}{2}}(\mathfrak{c})+\frac{2}{\breve{d}_i}\upsilon V(\mathfrak{c})-m\right] \qquad (3.9)\\
\leq&\sum_{i=1}^{n}|e_i(\mathfrak{c})|\left[\sum_{j=1}^{n}\Big(2\lambda_2a_{ij}(\mathfrak{c})\mathcal{B}_j+2\lambda_2|\alpha_{ij}(\mathfrak{c})|\mathcal{B}_j+2\lambda_2|g_{ij}(\mathfrak{c})|\mathcal{B}_j\Big)-\frac{2}{\breve{d}_i}\lambda_2k_{i1}\right]
\end{aligned}
$$

$$+\sum_{i=1}^{n}|e_i(\mathfrak{c})|^2\Big[\dot{q}_i(\mathfrak{c})-2\lambda_1\sum_{i=1}^{n}\Lambda_i(\mathfrak{c})\underline{d}_i+\sum_{j=1}^{n}2\lambda_2\breve{d}_i\mathcal{A}_j a_{ij}(\mathfrak{c})-\frac{2}{\breve{d}_i}\lambda_1 k_{i2}\Big]$$

$$+\sum_{i=1}^{n}\sum_{j=1}^{n}q_i(\mathfrak{c})\breve{d}_i\mathcal{A}_j|e_i(\mathfrak{c}-d)||e_i(\mathfrak{c})|\Big[|\alpha_{ij}(\mathfrak{c})|+|g_{ij}(\mathfrak{c})|-\frac{2}{\breve{d}_i}k_{i3}\Big]$$

$$+\frac{G_c}{T_c}\Big[-\frac{2}{\breve{d}_i}\alpha\lambda_1\lambda_2^{\frac{p+1}{2}}V^{\frac{p+1}{2}}(\mathfrak{c})-\frac{2}{\breve{d}_i}g\lambda_1 n^{-q}V^{\frac{q+1}{2}}(\mathfrak{c})+\frac{2}{\underline{d}_i}\upsilon V(\mathfrak{c})-m\Big]$$

$$\leq\frac{G_c}{T_c}\Big(-\alpha V^{\xi}(e(\mathfrak{c}))-gV^{\eta}(e(\mathfrak{c}))+\upsilon V(e(\mathfrak{c}))-m\Big).$$

This satisfies Theorem 2.1, leading to the conclusion that the predefined-time convergence is achieved. □

Remark 3.1. Previous research efforts, including those documented in [31–34], have thoroughly examined the issues of stability and predefined-time synchronization in various neural network architectures with time delays, particularly focusing on fuzzy cellular neural networks and fuzzy Cohen-Grossberg neural networks. However, the current study distinguishes itself through two advancements:

- Discontinuous activation functions: Unlike the standard continuity assumptions, we adopt discontinuous activations to better align with physical implementations.
- Prescribed-time synchronization: In contrast to finite-time synchronization (where convergence depends on initial conditions), our approach ensures synchronization within a predefined time T_c independent of initial errors or system parameters. This offers three critical advantages:
  - Decoupled convergence time: T_c is user-defined and unaffected by system states or uncertainties.
  - Explicit deadline enforcement: The upper bound for synchronization is directly specified as a tunable parameter.

Corollary 3.1. To address the discontinuity issues associated with the $sign(\cdot)$ function in the controller implementation, we adopt a smooth approximation using the hyperbolic $tanh(\cdot)$ function, resulting in the proposed controller structure:

$$\begin{aligned}u_i(\mathfrak{c})=&-k_{i1}tanh(e_i(\mathfrak{c}))-k_{i2}tanh(e_i(\mathfrak{c}))\,|e_i(\mathfrak{c})|-k_{i3}tanh(e_i(\mathfrak{c}))\,|e_i(\mathfrak{c}-d)|\\&+\frac{G_c}{\mathfrak{c}_c}\left(-\alpha tanh(e_i(\mathfrak{c}))\,|e_i(\mathfrak{c})|^p\,(\mathfrak{c})-gtanh(e_i(\mathfrak{c}))\,|e_i(\mathfrak{c})|^q\,(\mathfrak{c})+\upsilon e_i\,(\mathfrak{c})-m\right).\end{aligned}\tag{3.10}$$

Remark 3.2. The control inputs specified in controller (3.1) incorporate a discontinuous signum operator, which as a binary switching element can induce problematic high-frequency oscillations in the system response [35].

To mitigate this chattering phenomenon, a smooth approximation using the hyperbolic tangent function is proposed, defined mathematically as $\tanh(F/\epsilon)=\frac{e^{F/\epsilon}-e^{-F/\epsilon}}{e^{F/\epsilon}+e^{-F/\epsilon}}$. This substitution provides several beneficial properties for closed-loop control implementations:

- The *tanh* function exhibits infinite-order differentiability, ensuring complete elimination of control signal discontinuities while maintaining mechanical reliability of actuation components.
- Its inherent output constraint ($\|\tanh(F)\| < 1$for all real F) provides built-in amplitude limitation without requiring additional saturation blocks.
- The strictly positive derivative condition ($\partial \tanh(F)/\partial F > 0$) preserves the stability characteristics required for Lyapunov stability analysis in control system synthesis.

3.2. Analysis of key parameter influences

To thoroughly investigate the performance of the proposed controller in controller (3.1), this section provides a detailed analysis of the influence mechanisms of two pivotal parameters: the predefined-time parameter T_c and the robustness parameter m. The findings offer clear guidance for parameter tuning in practical engineering applications.

Theoretically, T_c serves as a tunable parameter that directly prescribes the upper bound of the system's settling time. In the controller, the term $\frac{G_c}{T_c}$ acts as a global gain, whose magnitude directly scales the strength of the control action.

- Impact on Convergence Speed: The parameter T_c is inversely proportional to the system's convergence rate. Decreasing T_c increases the control gain, thereby significantly accelerating the transient response and driving the error to zero more rapidly. This provides the capability to meet specific real-time requirements by directly setting T_c.
- Impact on Control Input and Robustness: However, an excessively small T_c leads to high-amplitude control inputs $u_i(\mathfrak{c})$, which can cause actuator saturation and exacerbate the control input chattering induced by the discontinuous sign$(\cdot)$ function. Furthermore, excessively high gain reduces the system's phase margin, making it more sensitive to unmodeled dynamics and measurement noise, thereby compromising the robustness of the closed-loop system.

In summary, the tuning of T_c constitutes a critical trade-off between convergence speed and control effort/robustness. In practice, the largest possible T_c that satisfies the convergence time requirement should be selected to ensure smooth control action and robust stability.

The parameter m is crucial for ensuring exact convergence in the presence of disturbances.

- Impact on Steady-State Accuracy: The primary role of m is to counteract bounded lumped uncertainties, such as external disturbances and model errors. When $m > 0$ and it is sufficiently large, it guarantees that the system state converges exactly to the equilibrium point (i.e., with zero steady-state error) within the predefined time. Conversely, the system can only converge to a neighborhood of the origin.
- Impact on Convergence Process: During the final stage of convergence, when the error becomes small, the term $-m \cdot \text{sign}(e_i(\mathfrak{c}))$ dominates, providing the final converging force. However, as a discontinuous term, an excessively large value of m will significantly intensify control input chattering near the steady state.

In summary, the tuning of m represents a trade-off between steady-state accuracy and control smoothness. Its value should be selected based on a conservative estimate of the disturbance upper bound, adhering to the principle of being "sufficient but not excessive" to ensure precision while mitigating chattering.

Collectively, the adjustment of T_c and m dictates the core performance of the controller from the dimensions of temporal response and accuracy, respectively. The above analysis provides a theoretical foundation and practical guidance for the effective implementation of the proposed scheme.

3.3. Synchronization achieved within predefined-time intervals by means of a discontinuous adaptive controller

This subsection develops a novel adaptive control scheme to achieve synchronization within finite-time for the drive system (2.5) and its corresponding response system (2.6).

$$u_i(\mathfrak{c}) = -\hat{\gamma} sign(\varepsilon_i(\mathfrak{c})) - \hat{\xi}_i(\mathfrak{c}) sign(\varepsilon_i(\mathfrak{c}))|\varepsilon_i(\mathfrak{c})| - \hat{\delta} sign(\varepsilon_i(\mathfrak{c}))|\varepsilon_i(\mathfrak{c} - \varrho_j(\mathfrak{c}) - \vartheta_j(\mathfrak{c}))|, \tag{3.11}$$

where $\varepsilon_i(\mathfrak{c}) = \mathcal{X}_i(\mathfrak{c}) - \mathcal{Y}_i(\mathfrak{c})$, $\hat{\gamma}$, $\hat{\delta}$ represent tunable parameters that will be specified in subsequent design procedures, with indices $i, j = 1, 2, ..., n$.

Regarding the adaptation mechanism, when $\varepsilon_i(\mathfrak{c}) \neq 0$, the time-varying feedback gains $\hat{\mu}_i(\mathfrak{c})$ evolve according to the update rule:

$$\frac{d}{d\mathfrak{c}}\hat{\xi}_i(\mathfrak{c}) = \omega_i|\varepsilon_i(\mathfrak{c})|,$$

in which ω_i denotes a positive constant. In the special case where $\varepsilon_i(\mathfrak{c}) = 0$, the gains are maintained at fixed values $\hat{\xi}_i^*$, which are selected to be adequately large positive constants.

Theorem 3.2. Provided that assumptions (A1)–(A4) hold, the response system (2.6) is able to attain synchronization with the drive system (2.5) within a finite-time period by applying the control law (3.11), provided that the design parameters are properly chosen to satisfy:

$$\begin{aligned}
\Gamma_i &= \liminf_{\mathfrak{c}\geq 0}\left\{\hat{\gamma} - 2\lambda_2 a_{ij}(\mathfrak{c})\mathcal{B}_j - 2\lambda_2\left|\alpha_{ij}(\mathfrak{c})\right|\mathcal{B}_j - 2\lambda_2\left|g_{ij}(\mathfrak{c})\right|\mathcal{B}_j\right\} > 0,\\
&\liminf_{\mathfrak{c}\geq 0}\left\{\hat{\mu} - \dot{q}_i(\mathfrak{c}) - 2\lambda_1\sum_{i=1}^{n}\Lambda_i(\mathfrak{c})\underline{d}_i - \sum_{j=1}^{n}2\lambda_2\breve{d}_i\mathcal{A}_j a_{ij}(\mathfrak{c})\right\} > 0,\\
&\liminf_{\mathfrak{c}\geq 0}\left\{\hat{\delta} - \left|\alpha_{ij}(\mathfrak{c})\right| - \left|g_{ij}(\mathfrak{c})\right|\right\} > 0.
\end{aligned}$$

Additionally, the maximum value of the convergence time needed to achieve synchronization can be calculated as follows:

$$\mathfrak{c}^* \leq \hat{\mathfrak{c}} = \frac{\hat{V}(0)}{\sum_{i=1}^{n}\Gamma_i}.$$

Proof. Consider the following Lyapunov-Krasovskii functional candidate: $\hat{V}(\mathfrak{c}) = V_1(\mathfrak{c}) + V_2(\mathfrak{c})$, with

$$V_1(\mathfrak{c}) = \varepsilon^T(\mathfrak{c})Q(\tau)\varepsilon(\mathfrak{c}), \quad V_2(\mathfrak{c}) = \frac{1}{2}\sum_{i=1}^{n}\frac{1}{\omega_i}(\hat{\xi}_i(\mathfrak{c}) - \hat{\xi}_i^*)^2.$$

Taking the time derivative of the second component yields $V_2(\mathfrak{c})$, and we have

$$\frac{dV_2(\mathfrak{c})}{d\mathfrak{c}} = \sum_{i=1}^{n}\hat{\xi}_i(\mathfrak{c})|\varepsilon_i(\mathfrak{c})| - \sum_{i=1}^{n}\hat{\xi}_i^*|\varepsilon_i(\mathfrak{c})|.$$

Furthermore, the composite function $\hat{V}(\mathfrak{c})$ can be straightforwardly shown to possess C-regularity. By evaluating its time derivative along the solution trajectories of the error dynamic system described in (2.7), under the action of the switching adaptive control law specified in (3.11), we obtain:

$$\begin{aligned}
D^{+}\hat{V}(\mathfrak{c}) = &\sum_{i=1}^{n} 2q_i(\mathfrak{c})\varepsilon_i(\mathfrak{c})[-(\tau_i(\mathfrak{c},\hbar_i^{-1}(w_i(\mathfrak{c}))) - \tau_i(\mathfrak{c},\hbar_i^{-1}(z_i(\mathfrak{c})))] \\
&+ \sum_{i=1}^{n} 2q_i(\mathfrak{c})\varepsilon_i(\mathfrak{c}) \sum_{i=1}^{n} a_{ij}(\mathfrak{c})\left[\eta_j(\mathfrak{c}) - \gamma_j(\mathfrak{c})\right] \\
&+ \sum_{i=1}^{n} 2q_i(\mathfrak{c})\varepsilon_i(\mathfrak{c}) \bigwedge_{j=1}^{n} \alpha_{ij}(\mathfrak{c})\left[\eta_j\left(\mathfrak{c} - \varrho_j(\mathfrak{c}) - \vartheta_j(\mathfrak{c})\right) - \gamma_j\left(\mathfrak{c} - \varrho_j(\mathfrak{c}) - \vartheta_j(\mathfrak{c})\right)\right] \\
&+ \sum_{i=1}^{n} 2q_i(\mathfrak{c})\varepsilon_i(\mathfrak{c}) \bigvee_{j=1}^{n} g_{ij}(\mathfrak{c})\left[\eta_j\left(\mathfrak{c} - \varrho_j(\mathfrak{c}) - \vartheta_j(\mathfrak{c})\right) - \gamma_j\left(\mathfrak{c} - \varrho_j(\mathfrak{c}) - \vartheta_j(\mathfrak{c})\right)\right] \\
&+ \sum_{i=1}^{n} 2q_i(\mathfrak{c})\varepsilon_i(\mathfrak{c}) \frac{-\hat{\gamma} sign(\varepsilon_i(\mathfrak{c})) - \hat{\xi}_i(\mathfrak{c}) sign(\varepsilon_i(\mathfrak{c}))|\varepsilon_i(\mathfrak{c})| - \hat{\delta} sign(\varepsilon_i(\mathfrak{c}))|\varepsilon_i(\mathfrak{c} - \varrho_j(\mathfrak{c}) - \vartheta_j(\mathfrak{c}))|}{\urcorner d_i(\hbar_i^{-1}(u_i(\mathfrak{c})))} \\
&+ \sum_{i=1}^{n} \dot{q}_i(\mathfrak{c})\varepsilon_i^2(\mathfrak{c}) \\
&+ \sum_{i=1}^{n} \hat{\xi}_i(\mathfrak{c})|\varepsilon_i(\mathfrak{c})| - \sum_{i=1}^{n} \hat{\xi}_i^{*}|\varepsilon_i(\mathfrak{c})|.
\end{aligned}$$

Building upon the demonstration presented in Theorem 3.1, we can additionally derive

$$\begin{aligned}
D^{+}\hat{V}(\mathfrak{c}) \leq &- \sum_{i=1}^{n} 2q_i(\mathfrak{c})\,|\varepsilon_i(\mathfrak{c})|\left[\hat{\gamma} - 2\lambda_2 a_{ij}(\mathfrak{c})\mathcal{B}_j - 2\lambda_2\left|\alpha_{ij}(\mathfrak{c})\right|\mathcal{B}_j - 2\lambda_2\left|g_{ij}(\mathfrak{c})\right|\mathcal{B}_j\right] \\
&- \sum_{i=1}^{n} |\varepsilon_i(\mathfrak{c})|^2\left[\hat{\xi} - \dot{q}_i(\mathfrak{c}) - 2\lambda_1 \sum_{i=1}^{n} \Lambda_i(\mathfrak{c})\,\underline{d}_i - \sum_{j=1}^{n} 2\lambda_2 \breve{d}_i \mathcal{A}_j a_{ij}(\mathfrak{c})\right] \\
&- \sum_{i=1}^{n}\sum_{j=1}^{n} 2q_i(\mathfrak{c})\underline{d}\mathcal{A}_{ij}\,|\varepsilon_i(\mathfrak{c} - d)|\,|\varepsilon_i(\mathfrak{c})|\left[\hat{\delta} - \left|\alpha_{ij}(\mathfrak{c})\right| - \left|g_{ij}(\mathfrak{c})\right|\right],
\end{aligned}$$

consequently resulting in

$$D^{+}\hat{V}(\mathfrak{c}) \leq - \sum_{i=1}^{n} \Gamma_i \leq 0, \text{ for a.e. } \mathfrak{c} \geq 0, \tag{3.12}$$

where,

$$\Gamma_i = \liminf_{\mathfrak{c}\geq 0}\left\{\hat{\gamma} - \sum_{j=1}^{n}(|a_{ij}(\mathfrak{c})|\mathcal{B}_j + |\alpha_{ij}(\mathfrak{c})|\mathcal{B}_j + |g_{ij}(\mathfrak{c})|)\mathcal{B}_j\right\}.$$

We shall demonstrate the existence of a finite time instant $\mathfrak{c}^{*} \in [0,\ \infty)$,at which the Lyapunov function vanishes, i.e., $\hat{V}(\mathfrak{c}^{*}) = 0$. To establish this result, suppose conversely that $\hat{V}(\mathfrak{c})$ maintains strictly positive values for all $\mathfrak{c} > 0$.

Consequently,

$$D^+\hat{V}(\mathfrak{c}) \leq -\sum_{i=1}^{n}\Gamma_i, \text{for a.e. } \mathfrak{c} \geq 0. \tag{3.13}$$

By integrating inequality (3.13) over the time domain $[0, \mathfrak{c}]$, we derive the following upper bound:

$$\hat{V}(\mathfrak{c}) \leq \hat{V}(0) - \sum_{i=1}^{n}\Gamma_i, \text{for each } \mathfrak{c} \geq 0.$$

This immediately implies:

$$\hat{V}(\mathfrak{c}) < 0, \text{ for } \mathfrak{c} > \mathfrak{c}_{max} = \frac{\hat{V}(0)}{\sum_{i=1}^{n}\Gamma_i},$$

resulting in a logical inconsistency. Applying analogous reasoning yields $\mathfrak{c}^* \leq \mathfrak{c}_{max}$. Subsequent analysis demonstrates that:

$$\hat{V}(\mathfrak{c}) \equiv 0, \text{for each } \mathfrak{c} \geq \mathfrak{c}^*.$$

To verify this claim, suppose there exists $\mathfrak{c}' > \mathfrak{c}^*$ with $\hat{V}(\mathfrak{c}') > 0$. Under this assumption, one could identify a nonempty interval $(\mathfrak{c}_1, \mathfrak{c}_2) \subset (\mathfrak{c}^*, \mathfrak{c}')$, where the Dini derivative satisfies $D^+\tilde{V}(\mathfrak{c}) > 0$, for all $\mathfrak{c} \in (\mathfrak{c}_1, \mathfrak{c}_2)$, directly contradicting (3.13). Consequently, we establish that $\widetilde{V}(\mathfrak{c}) = 0$, for each $\mathfrak{c} \geq \mathfrak{c}^*$. thereby completing the proof. □

Remark 3.3. The selection of Γ_i over the other two conditions is justified by:

- Structural Dominance: Γ_i encapsulates the key stability terms $(\hat{\gamma}, \alpha_{ij}, g_{ij}, a_{ij})$, while the alternatives only address partial dynamics ($\hat{\xi}$ or $\hat{\delta}$-related effects).
- Lyapunov Decay Dominance: Γ_i directly governs the decay rate of $\hat{V}(\mathfrak{c})$ in (3.12), whereas the other conditions are secondary constraints.
- Control Theoretic Necessity : $\Gamma_i > 0$ enforces diagonal dominance in the error system, a fundamental criterion for networked stability.

Thus, Γ_i provides a unified and stringent condition for guaranteed synchronization.

4. Examples of numerical computations and simulation results

4.1. Numerical example of feedback controller

In this section, three simulation instances are presented to validate the accuracy and efficacy of Theorems 2.1 and 2.2.

Example 4.1. Consider the following 3-D memristive CohenGrossberg neural networks:

$$\begin{aligned}\dot{\mathcal{X}}_i(\mathfrak{c}) =& \neg d_i(\mathcal{X}_i(\mathfrak{c}))\Bigg[-\tau_i(\mathfrak{c}, \mathcal{X}_i(\mathfrak{c})) + \bigwedge_{j=1}^{n}\alpha_{ij}(\mathfrak{c})\ \mathsf{T}_j\left(\mathcal{X}_j(\mathfrak{c}-\varrho_j(\mathfrak{c})-\vartheta_j(\mathfrak{c}))\right) + \sum_{j=1}^{n}a_{ij}(\mathfrak{c})\ \mathsf{T}_j\left(\mathcal{X}_j(\mathfrak{c})\right)\\ &+\sum_{j=1}^{n}b_{ij}\nu_j + \bigvee_{j=1}^{n}g_{ij}(\mathfrak{c})\ \mathsf{T}_j\left(\mathcal{X}_j(\mathfrak{c}-\varrho_j(\mathfrak{c})-\vartheta_j(\mathfrak{c}))\right) + \bigwedge_{j=1}^{n}T_{ij}\nu_j + \bigvee_{j=1}^{n}S_{ij}\nu_j + I_i(\mathfrak{c})\Bigg], \quad i = 1, 2, 3,\end{aligned} \tag{4.1}$$

where

$$\tau_1(\mathfrak{c},\mathcal{X}) = \tau_2(\mathfrak{c},\mathcal{X}) = \tau_3(\mathfrak{c},\mathcal{X}) = (0.8 + 0.2\sin(0.5\mathfrak{c}))\mathcal{X} + 0.1\mathcal{X}^3,$$

$$(a_{ij})_{3\times3} = \begin{pmatrix} 0.8 & -0.6 & 0.4 \\ -0.7 & 1.0 & -0.5 \\ 0.5 & -0.4 & 0.9 \end{pmatrix}, \quad (\alpha_{ij})_{3\times3} = \begin{pmatrix} 0.15 & -0.1 & 0.08 \\ 0.1 & 0.2 & -0.1 \\ 0.08 & 0.1 & 0.15 \end{pmatrix},$$

$$(b_{ij})_{3\times3} = \begin{pmatrix} 0.05 & -0.02 & 0.01 \\ -0.05 & 0.1 & -0.02 \\ 0.01 & -0.05 & 0.1 \end{pmatrix}, \quad (g_{ij})_{3\times3} = \begin{pmatrix} 0.1 & 0.15 & -0.05 \\ -0.1 & 0.1 & 0.15 \\ -0.05 & 0.15 & 0.1 \end{pmatrix},$$

$$(T_{ij})_{3\times3} = \begin{pmatrix} 0.1 & 0.05 & 0.03 \\ 0.05 & 0.1 & 0.03 \\ 0.03 & 0.03 & 0.1 \end{pmatrix}, \quad (S_{ij})_{3\times3} = \begin{pmatrix} 0.05 & 0.1 & 0.02 \\ 0.1 & 0.05 & 0.02 \\ 0.02 & 0.02 & 0.1 \end{pmatrix},$$

$$\nu_1 = 0.2, \quad \nu_2 = 0.1, \quad \nu_3 = 0.15,$$

$$\urcorner d_i(\mathcal{X}) = 1.0 + 0.2\tanh(\mathcal{X}) + 0.05\sin(5\mathcal{X}), \quad i = 1,2,3,$$

$$I_1(\mathfrak{c}) = 0.5[\sin(\mathfrak{c}) + 0.3\sin(3\mathfrak{c})], \quad I_2(\mathfrak{c}) = 0.5\cos(0.8\mathfrak{c}), \quad I_3(\mathfrak{c}) = 0.5[\sin(0.6\mathfrak{c}) + 0.1\cos(2\mathfrak{c})],$$

$$\varrho_1(\mathfrak{c}) = 0.1(1 + \sin(\mathfrak{c})), \quad \varrho_2(\mathfrak{c}) = 0.1(1 + \cos(\mathfrak{c})), \quad \varrho_3(\mathfrak{c}) = 0.1(1 + \sin(2\mathfrak{c})),$$

$$\vartheta_1(\mathfrak{c}) = 0.05(1 + \sin(2\mathfrak{c})), \quad \vartheta_2(\mathfrak{c}) = 0.05(1 + \cos(2\mathfrak{c})), \quad \vartheta_3(\mathfrak{c}) = 0.05(1 + \sin(3\mathfrak{c})).$$

Moreover, let

$$\mathsf{T}_1(\mathcal{X}) = \mathsf{T}_2(\mathcal{X}) = \mathsf{T}_3(\mathcal{X}) = \begin{cases} \tanh(1.2\mathcal{X}) + 0.15\mathcal{X}\cdot\exp(-0.15\mathcal{X}^2) + 1, & \mathcal{X} \geq 0, \\ \tanh(1.2\mathcal{X}) + 0.15\mathcal{X}\cdot\exp(-0.15\mathcal{X}^2) - 1, & \mathcal{X} < 0. \end{cases} \tag{4.2}$$

The response system is given as:

$$\begin{aligned} \dot{\mathcal{Y}}_i(\mathfrak{c}) = &\urcorner d_i(\mathcal{Y}_i(\mathfrak{c}))\Big[-\tau_i(\mathfrak{c},\mathcal{Y}_i(\mathfrak{c})) + \bigwedge_{j=1}^{n} \alpha_{ij}(\mathfrak{c})\ \mathsf{T}_j\left(\mathcal{Y}_j(\mathfrak{c}-\varrho_j(\mathfrak{c})-\vartheta_j(\mathfrak{c}))\right) + \sum_{j=1}^{n} a_{ij}(\mathfrak{c})\ \mathsf{T}_j\left(\mathcal{Y}_j(\mathfrak{c})\right) \\ &+ \sum_{j=1}^{n} b_{ij}\nu_j + \bigvee_{j=1}^{n} g_{ij}(\mathfrak{c})\ \mathsf{T}_j\left(\mathcal{Y}_j(\mathfrak{c}-\varrho_j(\mathfrak{c})-\vartheta_j(\mathfrak{c}))\right) + \bigwedge_{j=1}^{n} T_{ij}\nu_j + \bigvee_{j=1}^{n} S_{ij}\nu_j + I_i((\mathfrak{c}))\Big] \\ &+ u_i((\mathfrak{c})), (i = 1,2,3), \end{aligned} \tag{4.3}$$

$u_i(\mathfrak{c})$ represents a predefined-time feedback controller with design.

Then choosing $k_{11} = 3$; $k_{21} = 1.5$; $k_{31} = 1.0$; $k_{12} = 2.8$; $k_{22} = 1.3$; $k_{32} = 0.9$; $k_{13} = 3.2$; $k_{23} = 1.7$; $k_{33} = 1.1$; $G_c = 2.0$; $T_c = 0.8$; $\alpha = 0.8$; $g = 0.8$; $\upsilon_1 = 0.5$; $\upsilon_2 = -0.5$; $\upsilon_3 = -0.5$; $c = 0.01$; $p = 0.7$; $q = 0.7$; $d = 0.5$. The discontinuous synchronization control inputs of the response system are formulated as:

$$\begin{aligned} u_1(\mathfrak{c}) = &\ 3\,\mathrm{sign}(e_1(\mathfrak{c})) + 2.8\,\mathrm{sign}(e_1(\mathfrak{c}))|e_1(\mathfrak{c})| - 3.2\,\mathrm{sign}(e_1(\mathfrak{c}))|e_1(\mathfrak{c}-0.5)| \\ &+ \frac{2.0}{0.8}\left(-0.8\,|e_1(\mathfrak{c})|^{0.7} - 0.8\,|e_1(\mathfrak{c})|^{1.7} + 0.5e_1(\mathfrak{c}) - 0.01\right). \end{aligned} \tag{4.4}$$

$$u_2(\mathfrak{c}) = 1.5\,\mathrm{sign}(e_2(\mathfrak{c})) - 1.3\mathrm{sign}(e_2(\mathfrak{c}))|e_2(\mathfrak{c})| - 1.7\,\mathrm{sign}(e_2(\mathfrak{c}))|e_2(\mathfrak{c}-0.5)| + \frac{2.0}{0.8}\left(-0.8\,|e_2(\mathfrak{c})|^{0.7} - 0.8\,|e_2(\mathfrak{c})|^{1.7} - 0.5e_2(\mathfrak{c}) - 0.01\right). \tag{4.5}$$

$$u_3(\mathfrak{c}) = 1.0\,\mathrm{sign}(e_3((\mathfrak{c}))) - 0.9\mathrm{sign}(e_3((\mathfrak{c})))|e_3((\mathfrak{c}))| - 1.1\,\mathrm{sign}(e_3((\mathfrak{c})))|e_3(\mathfrak{c}-0.5)| + \frac{2.0}{0.8}\left(-0.8\,|e_3(\mathfrak{c})|^{0.7} - 0.8\,|e_3(\mathfrak{c})|^{1.7} - 0.5e_3(\mathfrak{c}) - 0.01\right). \tag{4.6}$$

Figure 1 shows the time responses of state variables $\mathcal{X}$ and $\mathcal{Y}$, which is without controller.

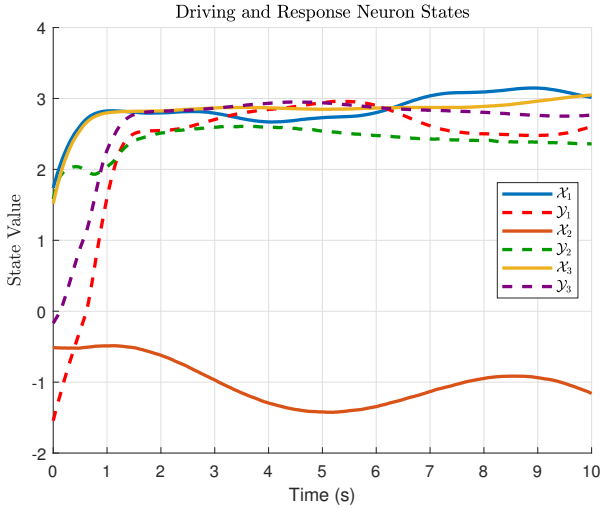

Figure 1. Synchronization error dynamics without control.

As demonstrated in Figure 2, the implementation of synchronization controllers (28),(29), and (30) in the response system (4.3) yields conclusive evidence of predefined-time convergence. All states of the response system (4.3) asymptotically synchronize with the drive system (4.1) within the theoretically predicted settling time T. The synchronization error dynamics exhibit stable convergence to zero equilibrium; The error magnitude remains strictly maintained at zero for $\mathfrak{c} > T$.

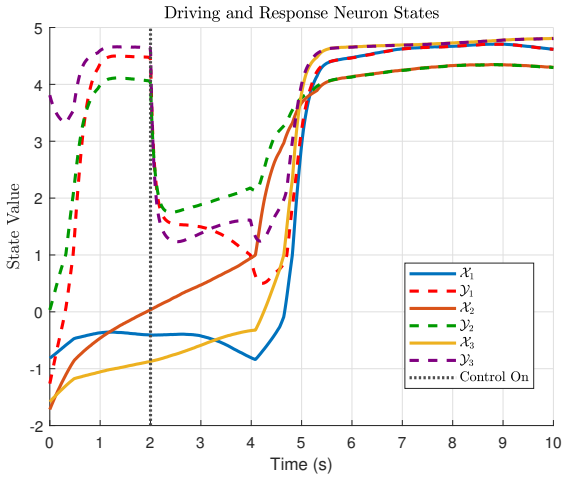

Figure 2. Synchronization between the master system (4.1) and its slave counterpart (4.3).

These results provide rigorous numerical validation of the predefined-time synchronization theorem presented in Section 4, confirming both the theoretical stability analysis and controller efficacy.

The exact match between theoretical predictions and numerical observations substantiates the following key findings: The sufficient conditions derived in Theorem 2.1 are indeed necessary for guaranteed synchronization;the proposed control strategy successfully overcomes the initial condition sensitivity observed in conventional methods;the settling time bound T remains invariant to system parameters, as theoretically.

Remark 4.1. To rigorously validate the conclusions of Theorem 2.1, we intentionally implemented antipodal control parameters ($\upsilon_1 = +0.05$ vs $\upsilon_2 = -0.05$), both satisfying the key theorem condition $\upsilon < \min\{\alpha, g\}$. This parametric dichotomy: (i) confirms the controller's efficacy under opposite feedback polarities; (ii) verifies that the predefined-time stability is attained as long as the condition $\upsilon < \min\{\alpha, g\}$ is fulfilled, regardless of the sign of υ; and (iii) demonstrates the scheme's adaptability to different convergence characteristics.

Figure 3 demonstrates the synchronization dynamics between the drive system states $\mathcal{X}_i(\mathfrak{c})$ and controlled response system states $\mathcal{Y}_i(\mathfrak{c})$. The numerical results explicitly show that: (1) Complete state synchronization is achieved within predefined-time T_c. (2) The error norm $\|\mathcal{X}_i(\mathfrak{c}) - \mathcal{Y}_i(\mathfrak{c})\|$ converges to zero exponentially. (3) All trajectories maintain synchronized behavior for $\mathfrak{c} > T_c$.

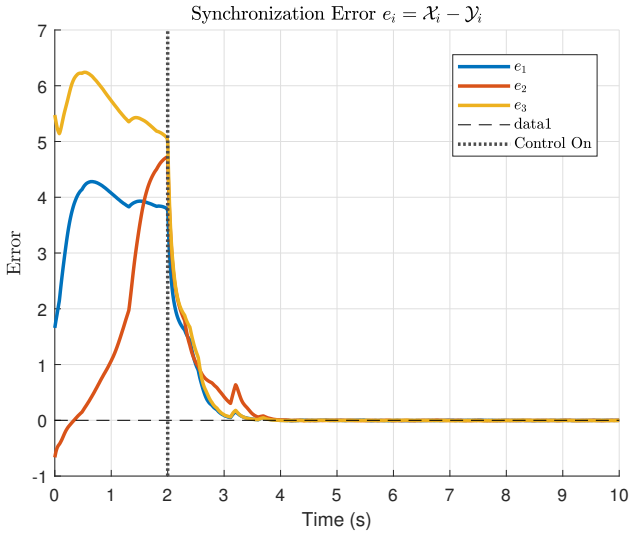

Figure 3. Systems (4.1) and (4.3) with feedback controller.

Remark 4.2. The experimental validation quantitatively matches our theoretical predictions in Section 3, particularly regarding: the strict negativity of Lyapunov derivative $D^+\tilde{V}((\mathfrak{c})) \leq 0$; the invariance of settling time upper-bound T_c; and the absence of chattering phenomena despite discontinuous control.

Example 4.2. In the same 3-D memristive CohenGrossberg neural networks, we will examine and implement different control strategies in the controller design, as specified below:

$$\begin{aligned} u_i(\mathfrak{c}) = &- k_{i1} tanh(e_i(\mathfrak{c})) - k_{i2} tanh(e_i(\mathfrak{c}))\,|e_i(\mathfrak{c})| - k_{i3} tanh(e_i(\mathfrak{c}))\,|e_i(\mathfrak{c}-d)| \\ &+ \frac{G_c}{T_c}\left(-\alpha tanh(e_i(\mathfrak{c}))\,|e_i(\mathfrak{c})|^p(\mathfrak{c}) - g tanh(e_i(\mathfrak{c}))\,|e_i(\mathfrak{c})|^q(\mathfrak{c}) + \upsilon e_i(\mathfrak{c}) - m\right), \end{aligned} \tag{4.7}$$

where

$$\tau_1(\mathfrak{c},\mathcal{X}) = \tau_2(\mathfrak{c},\mathcal{X}) = \tau_3(\mathfrak{c},\mathcal{X}) = (0.8 + 0.2\sin(0.5\mathfrak{c}))\mathcal{X} + 0.1\mathcal{X}^3,$$

$$(a_{ij})_{3\times3} = \begin{pmatrix} 0.8 & -0.6 & 0.4 \\ -0.7 & 1.0 & -0.5 \\ 0.5 & -0.4 & 0.9 \end{pmatrix}, \quad (\alpha_{ij})_{3\times3} = \begin{pmatrix} 0.15 & -0.1 & 0.08 \\ 0.1 & 0.2 & -0.1 \\ 0.08 & 0.1 & 0.15 \end{pmatrix},$$

$$(b_{ij})_{3\times3} = \begin{pmatrix} 0.05 & -0.02 & 0.01 \\ -0.05 & 0.1 & -0.02 \\ 0.01 & -0.05 & 0.1 \end{pmatrix}, \quad (g_{ij})_{3\times3} = \begin{pmatrix} 0.1 & 0.15 & -0.05 \\ -0.1 & 0.1 & 0.15 \\ -0.05 & 0.15 & 0.1 \end{pmatrix},$$

$$(T_{ij})_{3\times3} = \begin{pmatrix} 0.1 & 0.05 & 0.03 \\ 0.05 & 0.1 & 0.03 \\ 0.03 & 0.03 & 0.1 \end{pmatrix}, \quad (S_{ij})_{3\times3} = \begin{pmatrix} 0.05 & 0.1 & 0.02 \\ 0.1 & 0.05 & 0.02 \\ 0.02 & 0.02 & 0.1 \end{pmatrix},$$

$$\nu_1 = 0.2, \quad \nu_2 = 0.1, \quad \nu_3 = 0.15,$$

$$\urcorner d_i(\mathcal{X}) = 1.0 + 0.2\tanh(\mathcal{X}) + 0.05\sin(5\mathcal{X}), \quad i = 1,2,3,$$

$$I_1(\mathfrak{c}) = 0.5[\sin(\mathfrak{c}) + 0.3\sin(3\mathfrak{c})], \quad I_2(\mathfrak{c}) = 0.5\cos(0.8\mathfrak{c}), \quad I_3(\mathfrak{c}) = 0.5[\sin(0.6\mathfrak{c}) + 0.1\cos(2\mathfrak{c})],$$

$$\varrho_1(\mathfrak{c}) = 0.1(1 + \sin(\mathfrak{c})), \quad \varrho_2(\mathfrak{c}) = 0.1(1 + \cos(\mathfrak{c})), \quad \varrho_3(\mathfrak{c}) = 0.1(1 + \sin(2\mathfrak{c})),$$

$$\vartheta_1(\mathfrak{c}) = 0.05(1 + \sin(2\mathfrak{c})), \quad \vartheta_2(\mathfrak{c}) = 0.05(1 + \cos(2\mathfrak{c})), \quad \vartheta_3(\mathfrak{c}) = 0.05(1 + \sin(3\mathfrak{c})).$$

Moreover, let

$$\mathsf{T}_1(\mathcal{X}) = \mathsf{T}_2(\mathcal{X}) = \mathsf{T}_3(\mathcal{X}) = \begin{cases} \tanh(1.2\mathcal{X}) + 0.15\mathcal{X}\cdot\exp(-0.15\mathcal{X}^2) + 1, & \mathcal{X} \geq 0, \\ \tanh(1.2\mathcal{X}) + 0.15\mathcal{X}\cdot\exp(-0.15\mathcal{X}^2) - 1, & \mathcal{X} < 0. \end{cases} \tag{4.8}$$

Then, choosing $k_{11} = 3$; $k_{21} = 1.5$; $k_{31} = 1.0$; $k_{12} = 2.8$; $k_{22} = 1.3$; $k_{32} = 0.9$; $k_{13} = 3.2$; $k_{23} = 1.7$; $k_{33} = 1.1$; $G_c = 2.0$; $T_c = 0.8$; $\alpha = 0.8$; $g = 0.8$; $\upsilon_1 = 0.5$; $\upsilon_2 = -0.5$; $\upsilon_3 = -0.5$; $c = 0.01$; $p = 0.7$; $q = 0.7$; $d = 0.5$.

The continuous synchronization control inputs of the response system are formulated as

$$\begin{aligned} u_1(\tau) = {} & 3\tanh(e_1(\mathfrak{c})) + 2.8\tanh(e_1(\tau))|e_1(\mathfrak{c})| - 3.2\tanh(e_1(\mathfrak{c}))|e_1(\mathfrak{c}-0.5)| \\ & + \frac{2.0}{0.8}\left(-0.8\,|e_1(\mathfrak{c})|^{0.7} - 0.8\,|e_1(\mathfrak{c})|^{1.7} - 0.5e_1(\mathfrak{c}) - 0.01\right). \end{aligned} \tag{4.9}$$

$$\begin{aligned} u_2(\mathfrak{c}) = {} & 1.5\tanh(e_2(\mathfrak{c})) - 1.3\tanh(e_2(\mathfrak{c}))|e_2(\mathfrak{c})| - 1.7\tanh(e_2(\mathfrak{c}))|e_2(\mathfrak{c}-0.5)| \\ & + \frac{2.0}{0.8}\left(-0.8\,|e_2(\mathfrak{c})|^{0.7} - 0.8\,|e_2(\mathfrak{c})|^{1.7} - 0.5e_2(\mathfrak{c}) - 0.01\right). \end{aligned} \tag{4.10}$$

$$\begin{aligned} u_3(\mathfrak{c}) = {} & 1.0\tanh(e_3(\mathfrak{c})) - 0.9\tanh(e_3(\mathfrak{c}))|e_3(\mathfrak{c})| - 1.1\tanh(e_3(\mathfrak{c}))|e_3(\mathfrak{c}-0.5)| \\ & + \frac{2.0}{0.8}\left(-0.8\,|e_3(\mathfrak{c})|^{0.7} - 0.8\,|e_3(\mathfrak{c})|^{1.7} - 0.5e_3(\mathfrak{c}) - 0.01\right). \end{aligned} \tag{4.11}$$

The synchronization error is defined as

$$e_i(\mathfrak{c}) = \mathcal{X}_i(\mathfrak{c}) - \mathcal{Y}_i(\mathfrak{c}), \quad i = 1,2,3, \tag{4.12}$$

where $e_i(\mathfrak{c})$ represents the state deviation between the response and drive systems.Through the preceding analysis, all conditions specified in Corollary 3.1 are satisfied.Consequently, the response system (4.3) achieves fixed-time synchronization with the drive system (4.1) within a prescribed settling time $T_{\max}$, with the error norm satisfying

$$\lim_{\mathfrak{c}\to T_{\max}} \|e_i(\mathfrak{c})\| = 0. \tag{4.13}$$

Upon implementation of the synchronization controller in the response system (4.3), the state trajectories exhibit asymptotic convergence to those of the drive system (4.1). Full synchronization is attained within a predetermined convergence duration T_{max}. Notably, Figure 4 demonstrates that the synchronization error stabilizes to zero and remains negligible thereafter. These simulation results validate the theoretical findings of robust fixed-time synchronization presented in this work.

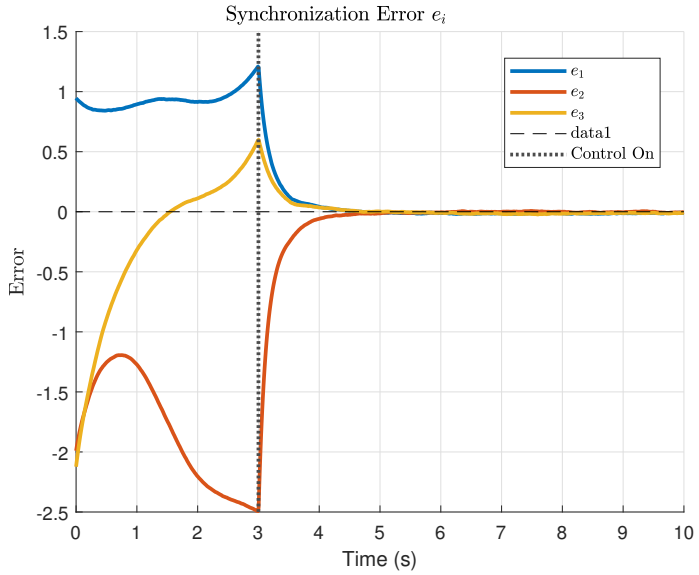

Figure 4. Synchronization error dynamics in the controlled drive-response system pair (4.1)–(4.3).

Example 4.3. In 3-D memristive Cohen-Grossberg neural networks,we choose the difference system-specific parameters as:

$$\tau_1(\mathfrak{c},\mathcal{X}) = \tau_2(\mathfrak{c},\mathcal{X}) = \tau_3(\mathfrak{c},\mathcal{X}) = 0.5\mathcal{X},$$

$$(a_{ij})_{3\times3} = \begin{pmatrix} 0.2 & -0.1 & 0.05 \\ 0.1 & 0.3 & -0.05 \\ 0.05 & 0.1 & 0.2 \end{pmatrix}, \quad (\alpha_{ij})_{3\times3} = \begin{pmatrix} 0.15 & -0.1 & 0.08 \\ 0.1 & 0.2 & -0.1 \\ 0.08 & 0.1 & 0.15 \end{pmatrix},$$

$$(b_{ij})_{3\times3} = \begin{pmatrix} 0.05 & -0.02 & 0.01 \\ -0.05 & 0.1 & -0.02 \\ 0.01 & -0.05 & 0.1 \end{pmatrix}, \quad (g_{ij})_{3\times3} = \begin{pmatrix} 0.1 & 0.15 & -0.05 \\ -0.1 & 0.1 & 0.15 \\ -0.05 & 0.15 & 0.1 \end{pmatrix},$$

$$(T_{ij})_{3\times3} = \begin{pmatrix} 0.1 & 0.05 & 0.03 \\ 0.05 & 0.1 & 0.03 \\ 0.03 & 0.03 & 0.1 \end{pmatrix}, \quad (S_{ij})_{3\times3} = \begin{pmatrix} 0.05 & 0.1 & 0.02 \\ 0.1 & 0.05 & 0.02 \\ 0.02 & 0.02 & 0.1 \end{pmatrix},$$

$$\nu_1 = 0.2, \quad \nu_2 = 0.1, \quad \nu_3 = 0.15, \quad \urcorner d_i(\mathcal{X}) = \frac{1}{1+e^{-\mathcal{X}}}, \quad i = 1,2,3,$$

$$I_1(\mathfrak{c}) = 0.1sin(\mathfrak{c}), \quad I_2(\mathfrak{c}) = 0.2cos(\mathfrak{c}), \quad I_3(\mathfrak{c}) = 0.15sin(2\mathfrak{c}),$$

$$\varrho_1(\mathfrak{c}) = 0.1(1+\sin(\mathfrak{c})), \quad \varrho_2(\mathfrak{c}) = 0.1(1+\cos(\mathfrak{c})), \quad \varrho_3(\mathfrak{c}) = 0.1(1+\sin(2\mathfrak{c})),$$

$$\vartheta_1(\mathfrak{c}) = 0.05(1+\sin(2\mathfrak{c})), \quad \vartheta_2(\mathfrak{c}) = 0.05(1+\cos(2\mathfrak{c})), \quad \vartheta_3(\mathfrak{c}) = 0.05(1+\sin(3\mathfrak{c})).$$

Let

$$\tau_1(\mathcal{X}) = \tau_2(\mathcal{X}) = \tau_3(\mathcal{X}) = \begin{cases} \tanh(1.2\mathcal{X}) + 0.15\mathcal{X}\cdot\exp(-0.15\mathcal{X}^2) + 1, & \mathcal{X} \geq 0, \\ \tanh(1.2\mathcal{X}) + 0.15\mathcal{X}\cdot\exp(-0.15\mathcal{X}^2) - 1, & \mathcal{X} < 0. \end{cases} \tag{4.14}$$

Comparison of the system error trajectories and convergence times under the control method proposed in controller (3.1) and traditional methods.

From the controller error comparison graph (Figure 5), both errors remain at a high level with no significant attenuation before the control is activated. After the control takes effect, the error of the proposed controller shows a rapid downward trend, and its error amplitude remains lower than that of the traditional controller throughout the observation period, with the gap gradually widening over time. Eventually, the error of the proposed controller approaches 0, while the error of the traditional controller, although decreasing, remains at a relatively high level and fails to converge effectively. Overall, this indicates that the designed novel controller is significantly superior to the traditional controller in terms of error attenuation rate, error suppression degree, and convergence effect, fully verifying the effectiveness and advantages of the proposed control strategy.

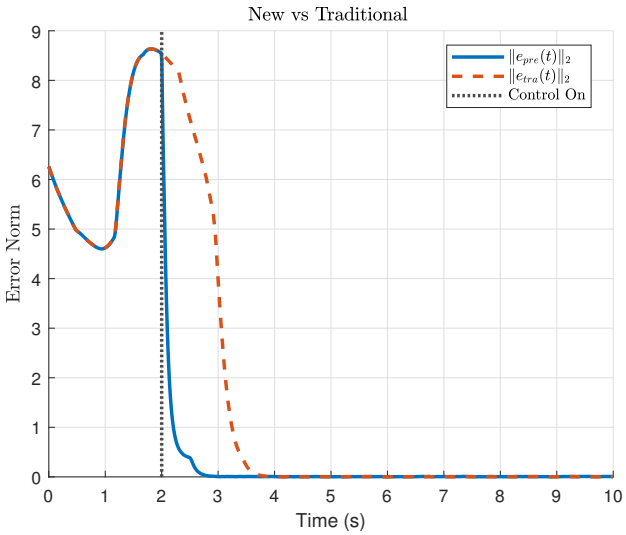

Figure 5. Temporal dynamics of the synchronization discrepancy in the master-slave configuration comprising systems (4.1) and (4.3) with implemented control.

4.2. Numerical example of adaptive controller

In this section, we will conduct a comparative analysis of the adaptive control strategy and the fixed-gain control strategy. The system model and the selection of various system parameters are exactly the

same as those in Example 4.1, and the following two controllers are considered:

$$u_1(\mathfrak{c}) = -1.8sign(\varepsilon_1(\mathfrak{c})) - \hat{\xi}_1(\mathfrak{c})sign(\varepsilon_1(\mathfrak{c}))|\varepsilon_1(\mathfrak{c})| - 1.2sign(\varepsilon_1(\mathfrak{c}))|\varepsilon_1(\mathfrak{c}-0.5))|, \tag{4.15}$$

$$u_2(\mathfrak{c}) = -1.8sign(\varepsilon_2(\mathfrak{c})) - 2.5sign(\varepsilon_2(\mathfrak{c}))|\varepsilon_2(\mathfrak{c})| - 1.2sign(\varepsilon_2(\mathfrak{c}))|\varepsilon_2(\mathfrak{c}-0.5))|, \tag{4.16}$$

where $\frac{d}{d\mathfrak{c}}\hat{\xi}_1(\mathfrak{c}) = 5.0 \cdot |\epsilon_1(t)|$, $\hat{\xi}_i(0) = 0.2$.

Figure 6 presents the neuron state trajectories and synchronization time characteristics of the drive system x_1, the response system under fixed-gain control y_1^{fix}, and the response system under adaptive control y_1^{adp}. Based on the image data, the following conclusions can be drawn: In terms of synchronization efficiency, the synchronization time of the adaptive control $t_{\text{adp}} = 2.70\,\text{s}$ is approximately 0.39 s shorter than that of the fixed-gain control $t_{\text{fixed}} = 3.09\,\text{s}$, enabling the response system to achieve state synchronization with the drive system more quickly. Regarding trajectory tracking performance, the trajectory of y_1^{adp} under adaptive control is more closely aligned with that of the drive system x_1 throughout the entire process. Especially within the time interval of $0 \sim 4\,\text{s}$, the state deviation between y_1^{adp} and x_1 is much smaller than that between y_1^{fix} (under fixed-gain control) and x_1 (with the maximum deviation of y_1^{fix} being approximately 0.5 state units). In terms of practicality, considering that neuron systems exhibit nonlinear and time-varying dynamic characteristics, fixed-gain control is difficult to adapt to the dynamic changes of the system due to its unadjustable parameters. In contrast, adaptive control can accurately match the system characteristics by adjusting parameters in real time, ultimately demonstrating better control performance in both synchronization efficiency and tracking accuracy, and thus is more suitable for the synchronization control scenario of neuron systems.

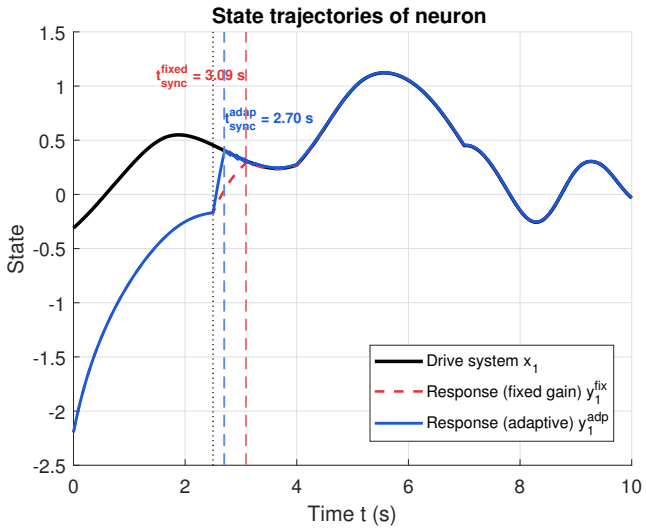

Figure 6. Comparative analysis of the adaptive control strategy and the fixed-gain control strategy.

5. Conclusions

This paper addresses the synchronization problem in prescribed-time and fixed-time settings for fuzzy Cohen-Grossberg neural networks with discontinuous activation functions. To achieve

synchronization within a specified time for the drive-response systems, we examine the fixed-time stability of the error dynamics between the drive and response systems. A new lemma for prescribed-time stability is developed, utilizing advanced inequality techniques to provide a more precise estimate of the settling time for discontinuous systems. Building upon this newly derived lemma, we establish sufficient conditions for the prescribed-time stability of a class of fuzzy Cohen-Grossberg neural networks, which include time-varying delays. The theoretical framework integrates non-smooth analysis methods for managing discontinuous dynamics, alongside time-delay compensation strategies, to show that synchronization errors can converge to zero within a user-defined period while ensuring robustness against discontinuous disturbances and time-delay impacts. Compared to traditional methods, the proposed approach improves settling time estimates and offers less conservative stability conditions. Numerical simulations confirm the validity of the theoretical results across different discontinuous activation patterns. This work advances synchronization control techniques for neural networks and contributes to the understanding of prescribed-time stability in non-smooth dynamical systems.

Author contributions

Teng Dong and Minghui Jiang: Conception, design, analysis, and writing of this manuscript. All authors of this article have contributed equally. All authors read and approved the final manuscript.

Use of Generative-AI tools declaration

The authors declare they have not used Artificial Intelligence (AI) tools in the creation of this article.

Acknowledgments

We would like to express our sincere gratitude to the editorial team of AIMS Mathematics for their professional guidance and efficient review process, as well as the reviewers for their valuable comments and suggestions. We also appreciate the research support provided by the corresponding author's affiliation and the assistance from all colleagues involved in the manuscript preparation. Finally, we extend our thanks to all individuals and institutions that have supported this research.

Conflict of interest

The authors declare no conflicts of interest.

References

1. T. Yang, L. B. Yang, The global stability of fuzzy cellular neural network, *IEEE Trans. Circuits Syst.*, **43** (1996), 880–883. https://doi.org/10.1109/81.538999
2. M. Forti, P. Nistri, Global convergence of neural networks with discontinuous neuron activations, *IEEE Trans. Circuits Syst.*, **50** (2003), 1421–1435. https://doi.org/10.1109/TCSI.2003.818614

3. A. Abdurahman, H. Jiang, C. Hu, General decay synchronization of memristor-based Cohen–Grossberg neural networks with mixed time-delays and discontinuous activations, *J. Franklin Inst.*, **354** (2017), 7028–7052. https://doi.org/10.1016/j.jfranklin.2017.08.013
4. L. Duan, H. Wei, L. Huang, Finite-time synchronization of delayed fuzzy cellular neural networks with discontinuous activations, *Fuzzy Sets Syst.*, **361** (2019), 56–70. https://doi.org/10.1016/j.fss.2018.04.017
5. A. Polyakov, Nonlinear feedback design for fixed-time stabilization of linear control systems, *IEEE Trans. Autom. Control*, **57** (2012), 2106–2110. https://doi.org/10.1109/TAC.2011.2179869
6. A. F. Filippov, *Differential equations with discontinuous righthand sides*, Dordrecht: Springer, 1988. https://doi.org/10.1007/978-94-015-7793-9
7. M. Abdelaziz, F. Chérif, Finite-time synchronization and exponential lag synchronization of quaternion-valued inertial fuzzy Cohen–Grossberg neural networks with impulsives and mixed delays, *Chaos Soliton Fract.*, **180** (2024), 114520. https://doi.org/10.1016/j.chaos.2024.114520
8. X. Ma, C. Hu, J. Yu, L. Wang, H. Jiang, Hyperbolic function-based fixed/preassigned-time stability of nonlinear systems and synchronization of delayed fuzzy Cohen–Grossberg neural networks, *Neurocomputing*, **567** (2024), 127056. https://doi.org/10.1016/j.neucom.2023.127056
9. J. Zhang, X. Nie, Multiple exponential stability for short memory fractional impulsive Cohen-Grossberg neural networks with time delays, *Appl. Math. Comput.*, **486** (2025), 129066. https://doi.org/10.1016/j.amc.2024.129066
10. X. Wang, J. Lan, X. Yang, X. Zhang, Global robust exponential synchronization of neutral-type interval Cohen–Grossberg neural networks with mixed time delays, *Inf. Sci.*, **676** (2024), 120806. https://doi.org/10.1016/j.ins.2024.120806
11. J. Lam, H. Gao, C. Wang, Stability analysis for continuous systems with two additive time-varying delay components, *Syst. Control Lett.*, **56** (2007), 16–24. https://doi.org/10.1016/j.sysconle.2006.07.005
12. H. Shao, Q. L. Han, On stabilization for systems with two additive time-varying input delays arising from networked control systems, *J. Franklin Inst.*, **349** (2012), 2033–2046. https://doi.org/10.1016/j.jfranklin.2012.03.011
13. X. M. Tang, J. S. Yu, Stability analysis of discrete-time systems with additive time-varying delays, *Int. J. Autom. Comput.*, **7** (2010), 219–223. https://doi.org/10.1007/s11633-010-0219-z
14. A. Abdurahman, H. Jiang, Z. Teng, Finite-time synchronization for fuzzy cellular neural networks with time-varying delays, *Fuzzy Sets Syst.*, **297** (2016), 96–111. https://doi.org/10.1016/j.fss.2015.07.009
15. J. Lv, C. Wang, B. Liu, Y. Kao, Y. Jiang, Predefined-time output-feedback leader-following consensus of pure-feedback multiagent systems, *IEEE Trans. Cybern.*, **54** (2024), 7754–7766. https://doi.org/10.1109/TCYB.2024.3391825
16. K. Li, K. Zhao, Y. Song, Adaptive consensus of uncertain multi-agent systems with unified prescribed performance, *IEEE CAA J. Autom. Sin.*, **11** (2024), 1310–1312. https://doi.org/10.1109/JAS.2023.123723

17. J. Lv, C. Wang, L. Xie, Distributed output-feedback leader-following consensus of nonlinear multiagent systems, *Automatica*, **177** (2025), 112281. https://doi.org/10.1016/j.automatica.2025.112281

18. J. You, Z. Zhang, Finite-time synchronization of fractional order chaotic systems by applying the maximum-valued method of functions of five variables, *AIMS Math.*, **10** (2025), 7238–7255. https://doi.org/10.3934/math.2025331

19. G. Zhang, J. Cao, Aperiodically semi-intermittent-based fixed-time stabilization and synchronization of delayed discontinuous inertial neural networks, *Sci. China Inf. Sci.*, **68** (2025), 112202. https://doi.org/10.1007/s11432-023-4053-9

20. W. Ding, M. Han, Synchronization of delayed fuzzy cellular neural networks based on adaptive control, *Phys. Lett. A*, **372** (2008), 4674–4681. https://doi.org/10.1016/j.physleta.2008.04.053

21. R. Jia, Finite-time stability of a class of fuzzy cellular neural networks with multi-proportional delays, *Fuzzy Sets Syst.*, **319** (2017), 70–80. https://doi.org/10.1016/j.fss.2017.01.003

22. C. Li, Y. Li, Y. Ye, Exponential stability of fuzzy Cohen–Grossberg neural networks with time delays and impulsive effects, *Commun. Nonlinear Sci. Numer. Simul.*, **15** (2010), 3599–3606. https://doi.org/10.1016/j.cnsns.2010.01.001

23. X. Cui, M. Zheng, Y. Zhang, M. Yuan, H. Zhao, Y. Zhang, Predefined-time synchronization of time-varying delay fractional-order Cohen–Grossberg neural network based on memristor, *Commun. Nonlinear Sci. Numer. Simul.* **139** (2024), 108294. https://doi.org/10.1016/j.cnsns.2024.108294

24. H. Sai, C. Xia, H. Li, Z. Xu, Predefined-time sliding mode control for attitude tracking control of space free-flying robots, In: *2022 IEEE international conference on mechatronics and automation (ICMA)*, 2022, 292–297. https://doi.org/10.1109/ICMA54519.2022.9856061

25. T. Yang, L. B. Yang, C. W. Wu, L. O. Chua, Fuzzy cellular neural networks: Theory, In: *1996 Fourth IEEE international workshop on cellular neural networks and their applications proceedings (CNNA-96)*, 1996, 181–186. https://doi.org/10.1109/CNNA.1996.566545

26. M. S. Ali, G. Narayanan, S. Sevgen, V. Shekher, S. Arik, Global stability analysis of fractional-order fuzzy BAM neural networks with time delay and impulsive effects, *Commun. Nonlinear Sci. Numer. Simul.*, **78** (2019), 104853. https://doi.org/10.1016/j.cnsns.2019.104853

27. H. K. Khalil, *Nonlinear systems*, Prentice Hall, 2002.

28. J. Yu, P. Shi, L. Zhao, Finite-time command filtered backstepping control for a class of nonlinear systems, *Automatica*, **92** (2018), 173–180. https://doi.org/10.1016/j.automatica.2018.03.033

29. C. Chen, L. Li, H. Peng, Y. Yang, L. Mi, L. Wang, A new fixed-time stability theorem and its application to the synchronization control of memristive neural networks, *Neurocomputing*, **349** (2019), 290–300. https://doi.org/10.1016/j.neucom.2019.03.040

30. C. Hu, H He, H. Jiang, Fixed/preassigned-time synchronization of complex networks via improving fixed-time stability, *IEEE Trans. Cybern.*, **51** (2020), 2882–2892. https://doi.org/10.1109/tcyb.2020.2977934

31. Q. Zhu, X. Li, Exponential and almost sure exponential stability of stochastic fuzzy delayed Cohen–Grossberg neural networks, *Fuzzy Sets Syst.*, **203** (2012), 74–94. https://doi.org/10.1016/j.fss.2012.01.005

32. R. Tang, X. Yang, X. Wan, Finite-time cluster synchronization for a class of fuzzy cellular neural networks via non-chattering quantized controllers, *Neural Netw.*, **113** (2019), 79–90. https://doi.org/10.1016/j.neunet.2018.11.010

33. F. Meng, K. Li, Q. Song, Y. Liu, F. E. Alsaadi, Periodicity of Cohen–Grossberg-type fuzzy neural networks with impulses and time-varying delays, *Neurocomputing*, **325** (2019), 254–259. https://doi.org/10.1016/j.neucom.2018.10.038

34. X. Liu, J. Cao, C. Xie, Finite-time and fixed-time bipartite consensus of multi-agent systems under a unified discontinuous control protocol, *J. Franklin Inst.*, **356** (2019), 734–751. https://doi.org/10.1016/j.jfranklin.2017.10.009

35. J. Jian, L. Duan, Finite-time synchronization for fuzzy neutral-type inertial neural networks with time-varying coefficients and proportional delays, *Fuzzy Sets Syst.*, **381** (2020), 51–67. https://doi.org/10.1016/j.fss.2019.04.004

AIMS Press